SIAM J. APPL. MATH.
Vol. 44, No. 2, April 1984

006

FINITE POLAR DIMPLING OF SHALLOW CAPS UNDER SUB-BUCKLING AXISYMMETRIC PRESSURE DISTRIBUTIONS*

DAVID F. PARKER† AND FREDERIC Y. M. WAN‡

Abstract. For shallow caps under an axisymmetric external pressure distribution which is inward (with a representative magnitude p_0) in a neighborhood of the pole and outward away from the pole, it has been shown previously that a finite axisymmetric dimple state of deformation is possible if p_0 is at least of the order of the classical buckling pressure for a complete spherical shell, p_c, and that, asymptotically, the corresponding dimple base is located by the condition of no resultant vertical force over the dimpled region. In the present paper, we treat the more difficult load magnitude range $p_0/p_c \ll 1$ by the method of inner-outer (asymptotic) expansions and show that there is a lower bound κ_c on p_0/p_c for the existence of a dimple state. For $p_0/p_c \geqq \kappa_c$, we derive a simple condition for the dimple base radius which reduces to the previous result when $(p_0/p_c)^{-1}$ is $O(1)$ at most. While the analysis is carried out for the special case of a quadratically varying pressure distribution, the method applies to more general load distributions with similar qualitative features, including a uniform internal pressure with an inward directed point force or ring load centered at the apex.

Key words. finite deformation shell theory, nonlinear elasticity, matched asymptotic expansions, interior layers

1. Introduction. Under favourable loading conditions, dome-shaped thin elastic shells of revolution are known to exhibit a predominantly inextensional bending deformation in the form of a finite axisymmetric dimple centered at the pole. For example, it has been shown in [1], [2] that polar dimpling is possible when a spherical shell is subject to an axisymmetric normal pressure distribution which is directed inward near a pole and outward in an adjacent region.[1] To a good approximation, the ***dimple base radius,*** which characterizes the location of the dimple base and therefore the dimple size, was shown to depend on the external loading in a simple way. To bring out the essential idea behind the asymptotic method for constructing the simple solution, results for a spherical cap with a clamped edge were first presented in [1] for a quadratically varying pressure distribution (see (1.1) below). Later, analogous and more general results were reported for a complete spherical shell in [2] for a sinusoidal pressure distribution.

Let $x\ (0 \leqq x \leqq 1)$ denote the dimensionless radial distance from the axis of revolution to a point on the middle surface of a clamped cap-like shallow shell of revolution having uniform thickness h. We consider here the polar dimpling problem of such a shell subjected to a general normal pressure distribution, $p(x) = p_e \hat{p}(x)$ with $|\hat{p}| \leqq 1$, ($\hat{p}$ is positive inward). We characterize the strength of the pressure loading by the parameter $\kappa = p_e/p_c$, where p_c denotes the classical buckling pressure for a spherical shell with the same radius of curvature at the pole. For the cap to behave

* Received by the editors July 14, 1981, and in revised form March 14, 1983. This research was partially supported by NSERC Operating Grants A9259 and A91 17.

† Department of Theoretical Mechanics, The University of Nottingham, Nottingham, NG7 2RD, England.

‡ Department of Mathematics and Institute of Applied Mathematics and Statistics, The University of British Columbia, Vancouver, British Columbia V6T 1 W5, Canada. The research of this author was supported by a UBC Killam Senior Fellowship.

[1] This type of load distribution is of interest to the designers of fuel containers for space crafts and to biomechanicians and physiologists interested in biological structures involving fluid-filled thin she[18], [19], [20].

as a shell (and not a flat plate), a parameter ε^2, which measures the thickness-to-rise ratio of the cap, must be small compared to unity. The polar dimpling problem for a shallow spherical cap and the specific pressure distribution,

$$p(x) = p_e(1 - c^2x^2) \qquad (c^2 > 1), \tag{1.1}$$

was treated in [1]. For $c^2 > 1$, the pressure distribution given by (1.1) is inward near the pole and outward near the shell edge. For such a pressure distribution, we see from the results in [1] that, when $\kappa\varepsilon$ is of order unity, one equilibrium configuration corresponds to an inextensional bending deformation except for narrow layers around the dimple base and adjacent to the cap edge. Furthermore, the dimple base location is determined to a good approximation by the positive root $x = \bar{x}_t$ of the equation

$$P(x) \equiv \frac{1}{p_e x}\int_0^x tp(t)\,dt = 0, \tag{1.2}$$

corresponding to a condition of no net axial force at the dimple base. In [1], this condition follows from the requirement that the radial stress resultant be continuous across the dimple base. For the loading **(1 .l),** we have $\bar{x}_t = \sqrt{2}/c$. Thus, the determination of the approximate dimensionless dimple base radius for our type of loading does not require an extra condition (e.g., minimum energy) beyond the elastostatics of the shell as it does in [3] for deep spherical shells under a point load (see also [4], [17] for spherical caps under a point load). In the language of singular perturbations, the inextensional bending solutions and the layer solutions correspond to the *outer* and *inner* asymptotic expansions, respectively, of the exact solution of the boundary value problem governing the elastostatics of the clamped spherical cap. The condition (1.2) effectively allows an approximate determination of the dimple base radius without any reference to the (nonelementary) *inner* solution(s) of the boundary value problem.

The approximate analysis of [1] is limited to the case of a spherical cap with a specific pressure loading and with $\kappa\varepsilon$ of order **unity.**[2] The analysis there avoids the final matching of the inner and outer solution and relies mainly on accurate numerical solutions of the original boundary value problem to confirm the accuracy of the dimple base location as determined by (1.2) and the adequacy of the outer solution away from the dimple base and shell edge. In this paper we obtain by the method of matched asymptotic expansions the corresponding polar dimpling solution for ***general*** cap-like shallow shells of revolution under more ***general*** axisymmetric loading conditions for a much wider range of p_e/p_c ratios. More specifically, when $\varepsilon^2 \ll 1$, we will show (for the first time) that polar dimpling is an admissible mode of deformation for $k_c\varepsilon \lesssim \kappa \ll \varepsilon^{-2}$, where k_c is a critical dimensionless number determined by the load and shell properties. For $\kappa \gg \varepsilon$ (but $\kappa\varepsilon = 0(1)$ or smaller), the condition $P(\bar{x}_t) = 0$ still gives a good first approximation $\bar{x}_t$ for the *dimensionless dimple base radius* x_T. For the important ("sub-buckling" applied pressure loading) range $k_c < \kappa/\varepsilon = \mathrm{O}(1)$, we will show that x_T is asymptotic to a root of the equation

$$4\kappa P(z) = \varepsilon I(z) \tag{1.3}$$

where $I(\cdot)$ is a function determined by the load and geometric properties of the shell and involving a pure number I_0 defined by the solution of a certain nonlinear boundary value problem. (For a spherical cap, $I(\cdot)$ takes the constant value I_0.) Thus, the

[2] With some trivial extensions of the technique used in [1], analogous results have been obtained for complete spherical shells with κ comparable to unity in [2]. The investigation reported there has obviously benefitted from the findings of the present research project as acknowledged in that report.

determination of the asymptotic dimple base radius for $\kappa/\varepsilon = O(1)$ is significantly (and qualitatively) different from the $\kappa \gg \varepsilon$ case and cannot be inferred from the latter. For example, dimpled solutions of various dimple sizes are now possible for a spherical cap with the quadratic load distribution (1.1) in the $\kappa/\varepsilon = O(1)$ range. Conveniently, solution of the boundary value problem (defined by (3.16), (3.17) and (4.3)) which determines I_0 also yields the leading term inner expansion for the bending layer for all $\kappa \ll \varepsilon^{-1}$, and so allows the construction of matched asymptotic expansions throughout this parameter range. At the other end of the load parameter range, we will show that, for $\kappa^{-1} = O(\varepsilon^2)$ the nonlinear membrane (instead of inextensional bending) action dominates *throughout* the cap.

These predictions are confirmed by accurate numerical solutions of the original boundary value problem, using the general boundary value problem solver COLSYS [5]. In all cases where there is a sharp dimple base, the asymptotic predictions are invaluable for efficient numerical computation. They provide accurate estimates of the location and thickness of the abrupt oscillatory changes which occur near the dimple base. Starting the iterative procedure from the inextensional bending solution with transition at the root $\bar{x}_t$ of (1.2), convergence to a numerical solution having prescribed error tolerance is obtained in many cases in which COLSYS would not otherwise have converged. Even with the help of the asymptotic results, careful parameter continuations are sometimes required to yield a dimple state solution. Without the asymptotic results, we could arrive at the erroneous conclusion that no dimpled state exists. It will also be shown that the condition (1.3), derived for the first time herein for the $\kappa = O(\varepsilon)$ load range, may be used to determine for $\varepsilon \ll \kappa \ll \varepsilon^{-2}$ a better approximation for the dimple base radius x_T than the leading term asymptotic expression $\bar{x}_t$. With this more accurate approximate dimple radius as an initial guess for COLSYS, parameter continuation is no longer necessary for most cases studied in this paper and accurate numerical solutions may be obtained efficiently, reducing the computing time required by the iterative scheme by one or two orders of magnitude from that required when $\bar{x}_t$ is used for x_T. Efficient and accurate numerical results for stresses and deformations in dimpled shells are important in design considerations.

Beyond their significant role in the numerical solution of the polar dimpling problem, our asymptotic results are also important from a theoretical viewpoint. They exhibit clearly the dependence of the existence, size and sharpness of a polar dimple, of the structure of the interior layer in the neighborhood of the dimple base, of the dominance of nonlinear membrane or bending shell action, etc. on the load and geometric properties of the shell. It is only through such a simple delineation (deduced for the first time herein) that we attain a good understanding of the qualitative features associated with the polar dimpling of cap-like shells of revolution. We do wish to emphasize however, that we are concerned only with the *possibility* of dimpled state(s) in this paper. Our analysis and computations show only that one (or more) dimpled state is a possible equilibrium configuration of a shallow cap for a certain range of the load and shell parameters. We do not attempt herein to determine loading histories which will lead to a dimpled state in preference to an undimpled state.

2. Formulation. The elastostatics of shells of revolution, which have undergone an axisymmetric finite deformation (with infinitesimal strain), may be formulated as a boundary value problem for a pair of coupled nonlinear second order ordinary differential equations for a stress function and a meridional slope variable [6]. With an undeformed meridional slope $\xi_0\Phi_0(x)$ $(\Phi_0(1) = 1)$ and a general axisymmetric (positive inward) normal load distribution $p = p_e\hat{p}(x)$ (with $|\hat{p}|_{\max} = 1$), we may take

these equations in the following dimensionless form [7]:

$$\varepsilon^2 x\left[\Psi''+\frac{1}{x}\Psi'-\frac{1}{x^2}\Psi\right]+\tfrac{1}{2}(\Phi^2-\Phi_0^2)=0, \tag{2.1}$$

$$\varepsilon^2 x\left[\Phi''+\frac{1}{x}\Phi'-\frac{1}{x^2}\Phi\right]-\Phi\Psi=4\kappa x P(x)+\varepsilon^2 x Q(x), \tag{2.2}$$

$$(0<x<1),$$

with

$$P(x)=\frac{1}{x}\int_0^x Q(t)\,dt, \tag{2.3}$$

$$Q(x)=\Phi_0''+\frac{1}{x}\Phi_0'-\frac{1}{x^2}\Phi_0. \tag{2.4}$$

In (2.1)–(2.4), a prime indicates differentiation with respect to x, $\xi_0\Phi(x)$ denotes the meridional slope of the deformed middle surface of the shell, and the dimensionless independent variable x is related to the radial distance from. the axis of revolution r $(0\leqq r\leqq r_0)$ by $x=r/r_0$ (see Fig. 1). In terms of r_0, the shell thickness h, Young's

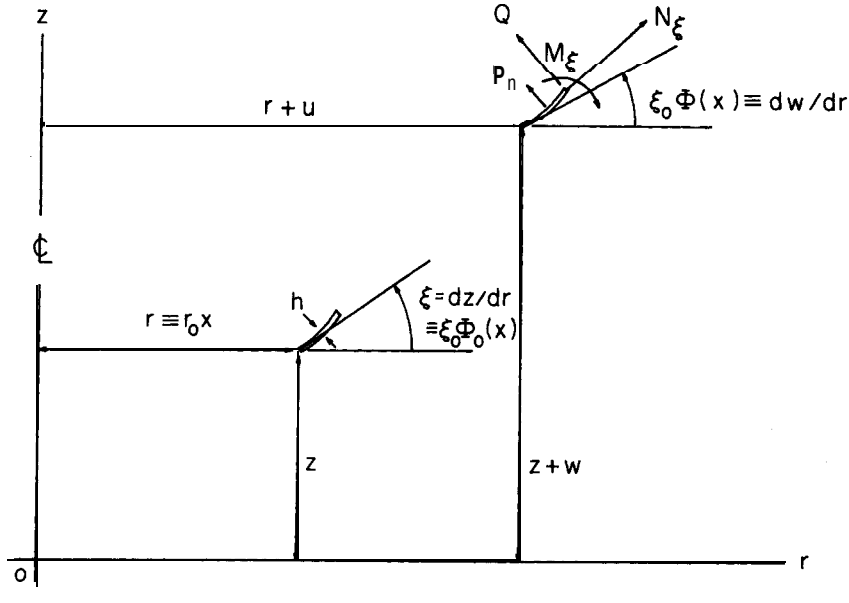

FIG. 1. Undeformed and deformed shell segments.

modulus E, Poisson's ratio ν, and the radius of curvature at the apex of the shell $a=r_0(\xi_0\Phi'(0))^{-1}$, we have

$$\varepsilon^2=\frac{ha}{2r_0^2\sqrt{3(1-\nu^2)}},\qquad \kappa=\frac{p_e}{p_c},\qquad p_c=\frac{2Eh^2}{a^2\sqrt{3(1-\nu^2)}}. \tag{2.5}$$

We note also that the dimensionless stress function Ψ is the conventional stress function normalized by $p_c a r_0/4$ with $p_c a\Psi/4x$ and $p_c a\Psi'/4$ being the radial and hoop stress resultants, respectively.

Equations (2.1) and (2.2) are supplemented by the regularity conditions at the apex:

$$x = 0: \quad \Phi = 0, \quad \Psi = 0, \tag{2.6}$$

and appropriate edge conditions depending on the type of support for the shell at $x = 1$. To be specific, we consider in this report only shells with a clamped edge so that

$$x = 1: \quad \Phi = 1, \quad \Psi' - \nu\Psi = 0, \tag{2.7}$$

though our analysis applies to shells with other types of edge support, possibly after suitable (but straightforward) modifications. The second condition in (2.7) corresponds to a requirement of no radial midsurface displacement. A discussion of other stress and deformation measures of the shallow shell can be found in [1], [2], [6]–[8].

For simplicity of presentation and for comparison with the results of [1], we shall first consider the simpler problem of a spherical cap ($\Phi_0(x) = x$) under a quadratically varying axisymmetric pressure load distribution (1.1). For this special case, the ODEs (2.1) and (2.2) become

$$\varepsilon^2 x\left[\Psi'' + \frac{1}{x}\Psi' - \frac{1}{x^2}\Psi\right] + \tfrac{1}{2}(\Phi^2 - x^2) = 0, \tag{2.8}$$

$$(0 < x < 1),$$

$$\varepsilon^2 x\left[\Phi'' + \frac{1}{x}\Phi' - \frac{1}{x^2}\Phi\right] - \Phi\Psi = 4\kappa x P(x). \tag{2.9}$$

After treating this special case in detail, we shall then discuss briefly how corresponding results can be similarly obtained for the more general problem.

3. **Inextensional bending solutions and interior layer analysis for the spherical cap.** Since the elevation of the edge of a cap above the base plane is

$$H = r_0\xi_0 \int_0^1 \Phi_0(x)\, dx,$$

the geometrical parameter ε^2 (defined in (2.5)) is proportional to the thickness-to-rise ratio. For the spherical cap, we have

$$\varepsilon^2 = \frac{h}{4H\sqrt{3(1-\nu^2)}}$$

A cap will exhibit shell action only if $h \ll H$; therefore, we will be concerned with the range $\varepsilon^2 \ll 1$ in this paper. For such a cap, the boundary value problem for Φ and Ψ has the structure associated with singular perturbation problems and a solution by the method of matched asymptotic expansions is appropriate. It is shown in [1] that, when κ is of order unity (so that p_e is large compared to the classical buckling load), the leading term outer solution corresponds to an inextensional deformation of dimple type. We anticipate that this type of outer solution is appropriate for a wider range of κ values and so, for each fixed value of κ, we take

$$\begin{aligned} &\Phi \sim -x\{1 + O(\varepsilon^2)\}, \qquad \Psi \sim 4\kappa P(x)\{1 + O(\varepsilon^2)\} \quad (0 \leqq x < x_T) \\ &\Phi \sim x\{1 + O(\varepsilon^2)\}, \qquad \Psi \sim -4\kappa P(x)\{1 + O(\varepsilon^2)\} \quad (x_T < x < 1) \end{aligned} \tag{3.1}$$

as the leading term outer solution of the differential equations (2.8) and (2.9) for some unknown (positive) *dimensionless dimple base radius* x_T defined by the criterion

$$\Phi(x_T) = 0 \qquad (0 < x_T < 1). \tag{3.2}$$

Adjacent to the edge $x = 1$ of the cap, Φ and Ψ exhibit a boundary layer behavior which reflects the effect of edge bending as the shell complies with the clamped edge condition (2.7). We shall not consider this aspect of the shell behavior henceforth as it is reasonably well-understood [6], [7], [8]. In general, another bending layer solution is needed around the dimple base to effect a smooth transition from one part of the inextensional solution (3.1) to the other. The stretched variable for this transition layer (or inner) solution may be taken in the form

$$x = x_T(\varepsilon; \kappa) + \lambda y \qquad (0 < \lambda \ll 1), \tag{3.3}$$

where A $\to 0$ as $\varepsilon \to 0$ and the dependence of x_T and A on ε (and κ) is to be chosen to allow for the existence of an inner solution which matches appropriately to the outer solution (3.1).

To determine x_T and A, we write the solution of (2.8) and (2.9) in terms of the "inner" variable y as

$$\Phi = x_T \phi(y, \varepsilon; \kappa), \qquad \Psi = \delta\psi(y, \varepsilon; \kappa), \tag{3.4}$$

where δ is another unknown scale factor and where (3.2) imposes the condition

$$\phi(0, \varepsilon; \kappa) = 0. \tag{3.5}$$

We stipulate that ϕ and ψ are $O(1)$ within the layer and that the first and second derivatives of ϕ and ψ with respect to y remain bounded as $\varepsilon \to 0$. We now write the two governing differential equations (2.8) and (2.9) in terms of ϕ, ψ and y:

$$\frac{\varepsilon^2}{\lambda^2}\delta(x_T + \lambda y)\left[\ddot{\psi} + \frac{\lambda}{x_T + \lambda y}\dot{\psi} - \frac{\lambda^2}{(x_T + \lambda y)^2}\psi\right] + \tfrac{1}{2}[x_T^2\phi^2 - (x_T + \lambda y)^2] = 0, \tag{3.6}$$

$$\begin{aligned}&\frac{\varepsilon^2}{\lambda^2}x_T(x_T + \lambda y)\left[\ddot{\phi} + \frac{\mathrm{A}}{x_T + \lambda y}\dot{\phi} - \frac{\lambda^2}{(x_T + \lambda y)^2}\phi\right] - x_T\delta\phi\psi \\ &\quad = 4\kappa(x_T + \lambda y)P(x_T + \lambda y) = K(x_T + \lambda y)^2[2 - c^2(x_T + \lambda y)^2],\end{aligned} \tag{3.7}$$

where a dot indicates differentiation with respect to y. One condition on the choice of the parameters A, δ and x_T follows immediately from a balance of terms in (3.6):

$$\frac{\varepsilon^2}{\lambda^2}\delta x_T = x_T^2 \tag{3.8}$$

giving the distinguished limit [9], [10]

$$\ddot{\psi}_0 + \tfrac{1}{2}(\phi_0^2 - 1) = 0 \tag{3.9}$$

of (3.6) (or (2.8)), with

$$\psi_0 = \psi(y, 0; \kappa), \qquad \phi_0 = \phi(y, 0; \kappa).$$

(i) $\varepsilon \ll K \ll \varepsilon^{-1}$. When κ is $O(1)$, a distinguished limit for (3.7) is obtained by setting

$$\frac{\varepsilon^2}{\lambda^2}x_T^2 = \delta x_T$$

which, together with (3.8), implies

$$\delta = x_T, \quad \mathrm{A} = \varepsilon. \tag{3.10}$$

The limiting form of (3.7) in this case is

$$\ddot{\phi}_0 - \phi_0\psi_0 = b \equiv \frac{4\kappa}{x_t}P(x_t), \tag{3.11}$$

where

$$x_t = x_t(\kappa) \equiv \lim_{\varepsilon\to 0} x_T(\varepsilon;\kappa). \tag{3.12}$$

The system (3.9) and (3.11), supplemented by suitable auxiliary conditions, determines the leading term inner solution (ϕ_0, ψ_0) with x_t as an unknown parameter. Since ϕ_0 and ψ_0 must match with the leading term outer solution (3.1), appropriate auxiliary conditions are deduced from the matching to be

$$y \to \pm\infty: \quad \phi_0 \to \pm 1, \quad \psi_0 \to \mp b \tag{3.13}$$

(with $\dot{\phi}_0 \to 0$ and $\dot{\psi}_0 \to 0$).

The boundary value problem (3.9), (3.11) and (3.13) does not always have a solution. To see this, we note that the two differential equations (3.9) and (3.11) have a first integral which can be deduced in the usual way (first multiplying (3.9) and (3.11) by $\dot{\psi}_0$ and $\dot{\phi}_0$ respectively, forming the difference of the two resulting equations and then integrating):

$$\begin{aligned} 0 &= \int_{-\infty}^{y} \{[\ddot{\psi}_0 + \tfrac{1}{2}(\phi_0^2 - 1)]\dot{\psi}_0 - [\ddot{\phi}_0 - \phi_0\psi_0 - b]\dot{\phi}_0\}\, dy \\ &= \tfrac{1}{2}[\dot{\psi}_0^2 - \dot{\phi}_0^2 + (\phi_0^2 - 1)\psi_0 + 2b\phi_0]_{-\infty}^{y}. \end{aligned} \tag{3.14}$$

Letting $y \to \infty$ and applying the matching conditions (3.13) then lead to $2b = 0$. Consequently, we must have

$$\frac{4K}{x_t}P(x_t) = \kappa(2 - c^2 x_t^2) = 0$$

in order for the boundary value problem for ϕ_0 and ψ_0 to have a solution. This implies that for $\varepsilon^2 \ll \kappa\varepsilon \ll 1$, the leading term expression for the dimensionless dimple radius $x_T(>0)$ is $x_T \sim x_t$ just as in the case $\varepsilon \ll \kappa\varepsilon = O(1)$ investigated in [1], but now as a consequence of the existence of a layer solution in the context of matched asymptotic expansions. In the case of the quadratically varying pressure distribution (1.1), we get

$$x_T \sim x_t = \sqrt{2}/c \equiv \bar{x}_t. \tag{3.15}$$

Then, setting $b = 0$ in (3.11) and (3.13), we express the leading term approximations to the transition layer solution $\phi(y)$ and $\psi(y)$ by the solution $\phi_0 = v(y), \psi_0 = w(y)$ to the system

$$\ddot{w} - \tfrac{1}{2}(1 - v^2) = 0, \quad \ddot{v} - vw = 0, \tag{3.16}$$

$$y \to \pm\infty: \quad w \to 0, \quad v \to \pm 1, \qquad v(0) = 0. \tag{3.17}$$

The condition $v(0) = 0$ in (3.17) follows from the defining conditions (3.2)–(3.4) and the definition of v(y).

The system (3.16) and (3.17), with x_T given by (3.15), determines the leading term transition (inner) solution when $\varepsilon \ll \kappa = 0(1)$. Moreover, since we may write[3]

$$4\kappa\,(x_T + \varepsilon y)P(x_T + \varepsilon y) = 4\kappa x_t P(x_t) + O(\kappa\varepsilon)$$

[3] The condition $x_T - x_t = O(\varepsilon)$ needed for this step is deduced later in § 4.

at each finite y, we deduce that the system (3.16), (3.17) and the expression (3.15) for the limiting dimensionless dimple radius x_t hold *throughout* the range $\varepsilon \ll \kappa \ll \varepsilon^{-1}$. Evidently, the completely inverted cap is the only dimple state when $c \leqq \sqrt{2}$.

We note that, if the condition $v(0)=0$ were absent, the boundary value problem (3.16), (3.17) possesses a whole equivalence class of solutions $(v(y+c), w(y+c))$ obtained from one solution $(v(y), w(y))$ by a translation $y \to y+c$ (c finite) just as in the transition layer analyzed by Fife [11]. Although we have not proved either existence or uniqueness of solutions to the boundary value problem (3.16), (3.17), we see that (3.17) (including $v(0)=0$) is compatible with the choice of $v(y)$ and $w(y)$ as respectively, odd and even functions. Only one solution with these properties has been obtained over the range $0 \leqq y < \infty$ numerically, using the general BVP solver COLSYS with the boundary conditions $v(0)=0$, $\dot{w}(0)=0$ and $w(0)=-\dot{v}^2(0)$, which follows from (3.14). Henceforth we shall assume that $v(y)$ and $w(y)$ correspond to this solution.

(ii) $\kappa = O(\varepsilon)$. When κ is comparable with ε, the expression b is $O(\varepsilon)$ and should not appear in (3.11) and (3.13). Consequently, the vanishing of the first integral (3.14) as $y \to \infty$ imposes no restriction on x_t. The determination of x_t in this case cannot be deduced from the leading term solution. It constitutes a main result of this paper and will be discussed in § 4. Moreover, the procedure developed in that section provides a unified method for calculating the difference $x_T - \bar{x}_t$ throughout the range $\varepsilon \ll \kappa \ll \varepsilon^{-1}$.

(iii) $\varepsilon \ll \kappa\varepsilon = O(1)$. In this range, the dimple location is still given by (3.15) but $\kappa P(x)$ is not negligible within the transition layers [1]. Terms of order $\kappa\varepsilon$ should be retained in the limit equation derived from (3.7):

$$\ddot{\phi}_0 - \phi_0\psi_0 = \alpha - \beta y \tag{3.18}$$

where

$$\alpha = \lim_{\varepsilon \to 0} 4\kappa x_T^{-1} P(x_T),$$

$$\beta = \lim_{\varepsilon \to 0} [-4\kappa\varepsilon x_T^{-1} P'(x_T)] = 4\kappa\varepsilon/\bar{x}_t = 2\sqrt{2}\,\kappa\varepsilon c,$$

both limits being taken with $\kappa\varepsilon$ held fixed. This is to be solved together with (3.9) and the matching conditions:

$$y \to \pm\infty: \quad \phi_0 \to \pm 1, \quad \psi_0 \to \pm(\beta y - \alpha). \tag{3.19}$$

In this case, multiplication by $\dot{\psi}_0$ and $\dot{\phi}_0$ followed by integration does not yield a restriction on α. This is hardly surprising since, if the pair $V(y;\beta)$ and $W(y;\beta)$ is a solution of the system

$$\ddot{W} - \tfrac{1}{2}(1 - V^2) = 0, \qquad \ddot{V} - VW = -\beta y, \tag{3.20}$$

$$y \to \pm\infty: \quad V \to \pm 1, \quad W \to \pm\beta y, \tag{3.21}$$

then the pair $\phi_0 = V(y + \alpha/\beta; \beta)$ and $\psi_0 = W(y + \alpha/\beta; \beta)$ is a solution of the boundary value problem (3.9), (3.18) and (3.19). A variation of the parameter α corresponds merely to a finite translation along the y-axis (corresponding to an $O(\varepsilon)$ shift in x). However, the criterion $\Phi(x_T)=0$ in (3.2) gives $\phi_0(0)=0$ which provides a restriction on α since we would expect that the nonlinear boundary value problem (3.20), (3.21) to possess at most a finite number of solutions, with each V having only a finite number of zeros. Although we claim nothing about uniqueness (see [11]), we select the solution (V, W) in which V is an odd function and W an even function of y. Since

we have $V(0)=0$ in this solution, we deduce $\alpha = 0$ so giving

$$P(x_T) = o(\kappa^{-1}) = o(\varepsilon)$$

and leading to

$$x_T = \bar{x}_t + o(\varepsilon)$$

with

$$\phi_0 = V(y;\beta), \qquad \psi_0 = W(y;\beta).$$

(iv) $1 \ll \kappa\varepsilon \ll \varepsilon^{-1}$. When $\kappa\varepsilon \gg 1$, the choice of (3.10) for the scale factors δ and A is no longer appropriate. Inspection of (3.7) suggests that we replace (3.10) by

$$x_T\delta = \kappa\lambda x_T^2, \qquad P(x_T) = O(\lambda),$$

which, together with (3.8), leads to the scaling

$$\lambda = \kappa\varepsilon^2, \qquad \delta = \kappa^2\varepsilon^2 x_T.$$

In order to have $A \ll 1$, we require $\varepsilon^{-1} \ll \kappa \ll \varepsilon^{-2}$ and the distinguished limits for (3.6) and (3.7) then are (3.9) and

$$\phi_0\psi_0 = \gamma y - \alpha$$

where

$$\alpha = \lim_{\varepsilon\to 0} 4x_T^{-1}\lambda^{-1}P(x_T),$$

$$\gamma = \lim_{\varepsilon\to 0} [-4x_T^{-1}P'(x_T)] = 4/\bar{x}_t = 2\sqrt{2}\,c.$$

The appropriate matching conditions are

$$y \to \pm\infty: \quad \phi_0 \to \pm 1, \quad \psi_0 \to \pm(\gamma y - \alpha).$$

Again, we take the solution (ϕ_0, ψ_0) to be an odd function $\bar{V}(y;\gamma)$ and an even function $\bar{W}(y;\gamma)$, respectively, which satisfy

$$\bar{W}'' - \tfrac{1}{2}(1 - \bar{V}^2) = 0, \qquad \bar{V}\bar{W} = \gamma y, \tag{3.22}$$

$$y \to \pm\infty: \quad \bar{V} \to \pm 1, \quad \bar{W} \to \pm\gamma y. \tag{3.23}$$

In this case, we have

$$y = \frac{x - x_T}{\kappa\varepsilon^2}, \qquad \Psi = \kappa^2\varepsilon^2 x_T\psi \sim \kappa^2\varepsilon^2 x_T\bar{W}(y), \tag{3.24}$$

while the criterion $\Phi(x_T) = 0$ shows that $\alpha = 0$ so that $x_T = \bar{x}_t + o(A) = \bar{x}_t + o(\kappa\varepsilon^2)$.

The system (3.22), (3.23) is equivalent to a single second order equation for $\bar{W}(y)$. Its order is lower than the systems describing the transition behavior in other ranges of κ values, but it is still capable of describing a transition between the two inextensional bending solutions (3.1). The transition has the structure of a nonlinear membrane deformation [8] and the transition layer width is greater than in the previous cases, being comparable with $\kappa\varepsilon^2 (\gg \varepsilon)$.

As $\kappa\varepsilon^2$ increases to become comparable with unity (or larger) the width of the membrane transition becomes comparable with the radius of the cap. No transition layer of dimple type can be expected in this case. Indeed, for $\kappa^{-1} = O(\varepsilon^2)$ the

appropriate scaling of (2.8) and (2.9) is (see [17])

$$\Psi=(\kappa/\varepsilon)^{2/3}\hat{\Psi},\qquad \Phi=(\kappa\varepsilon^2)^{1/3}\hat{\Phi},$$

which gives $\hat{\Psi}_0$ and $\hat{\Phi}_0$ as the leading order approximation of the outer solution for Ψ and Φ with

$$x\left[\hat{\Psi}_0''(x)+\frac{1}{x}\hat{\Psi}_0'(x)-\frac{1}{x^2}\hat{\Psi}_0(x)\right]+\tfrac{1}{2}(\hat{\Phi}_0^2-(\kappa\varepsilon^2)^{-2/3}x^2)=0$$
$$\hat{\Phi}_0\hat{\Psi}_0=-4xP(x). \qquad (0<x<1),$$

These equations describe a nonlinear membrane behavior throughout the cap$0<x<1$, with a deformed slope $\hat{\Phi}_0(x)$ which is sensitive to all details of $P(x)$.

In summary and for the purpose of a composite expansion, we note that for all $\varepsilon\ll\kappa\ll\varepsilon^{-2}$ the leading order approximation to the dimple base location is $x_T\sim\bar{x}_t=\sqrt{2}/c$. For $\varepsilon\ll\kappa=O(\varepsilon^{-1})$ an appropriate inner variable is $y\equiv(x-x_T)/\varepsilon$, with leading order inner expansions

$$\begin{aligned}&\Phi\sim x_T v(y), && \Psi\sim x_T w(y) && (\varepsilon\ll\kappa\ll\varepsilon^{-1}),\\ &\Phi\sim x_T V(y;\beta), && \Psi\sim x_T W(y;\beta) && (\kappa=O(\varepsilon^{-1})),\end{aligned}\tag{3.25}$$

with $\beta\equiv 2\sqrt{2}\,\kappa\varepsilon c=4\kappa\varepsilon/\bar{x}_t$. Here the odd function $V(y;\beta)$ and even function $W(y;\beta)$ solve the boundary value problem (3.20), (3.21). The pair of functions $v(y)$, w(y) given by (3.16), (3.17) are just the limiting functions

$$v(y)=\lim_{\kappa\varepsilon\to 0}V(y;4\kappa\varepsilon/\bar{x}_t),\qquad w(y)=\lim_{\kappa\varepsilon\to 0}W(y;4\kappa\varepsilon/\bar{x}_t).\tag{3.26}$$

The inner expansions may be combined with the leading term outer solution (3.1) in the usual way to form the composite expansion

$$\begin{aligned}&\phi\sim(x_T-x)+x_TV(y;\beta),\quad \psi\sim 4\kappa[P(x)+x-x_T]+x_TW(y;\beta)\quad (0\leqq x<x_T)\\ &\phi\sim(x-x_T)+x_TV(y;\beta),\quad \psi\sim -4\kappa[P(x)+x-x_T]+x_TW(y;\beta)\quad (x_T<x<1).\end{aligned}\tag{3.27}$$

For larger values of κ ($1\ll\kappa\varepsilon\ll\varepsilon^{-1}$), the composite expansion (3.27) is still valid but the parameter $\beta=4\kappa\varepsilon/\bar{x}_t$ is large. The leading term inner expansion is determined more simply by use of the scaling (3.24) with $x_T=\bar{x}_t+O(\kappa\varepsilon^2)$. It may be written in terms of the odd function $\bar{V}(y)$ and even function $\bar{W}(y)$ which solve the boundary value problem (3.22), (3.23) and which are given alternatively as

$$\bar{V}\left(\frac{x-x_T}{\kappa\varepsilon^2}\right)=\lim_{\kappa\varepsilon\to\infty}V\left(\frac{x-x_T}{\varepsilon};\frac{4\kappa\varepsilon}{\bar{x}_t}\right),\quad \bar{W}\left(\frac{x-x_T}{\kappa\varepsilon^2}\right)=\frac{1}{\kappa^2\varepsilon^2}\lim_{\kappa\varepsilon\to\infty}W\left(\frac{x-x_T}{\varepsilon};\frac{4\kappa\varepsilon}{\bar{x}_t}\right).\tag{3.28}$$

The composite expansion (3.27) is then simplified by replacing $V(y;\beta)$ and $W(y;\beta)$ by $\bar{V}((x-x_T)/\kappa\varepsilon^2)$ and $\kappa^2\varepsilon^2\bar{W}((x-x_T)/\kappa\varepsilon^2)$, respectively. We note also that any of the composite expansions may be replaced by an equivalent multiplicative representation $\Phi\sim xV(y;4\kappa\varepsilon/\bar{x}_t)$.

The results of the above asymptotic analysis for the range $\varepsilon\ll\kappa\ll\varepsilon^{-2}$ have been confirmed by accurate numerical solutions of the original boundary value problem (2.5)–(2.9). In addition to those reported in [1], [2], [12], [17] distributions of $\Phi(x)$ are plotted in Figs. 2 and 3 to show the effect of several parameters. All numerical results reported herein are for $\nu=0.3$ and generated by the boundary value problem solver COLSYS [5] which is a general purpose computer code for solving ordinary differential equations with prescribed boundary values at the end (and/or intermediate)

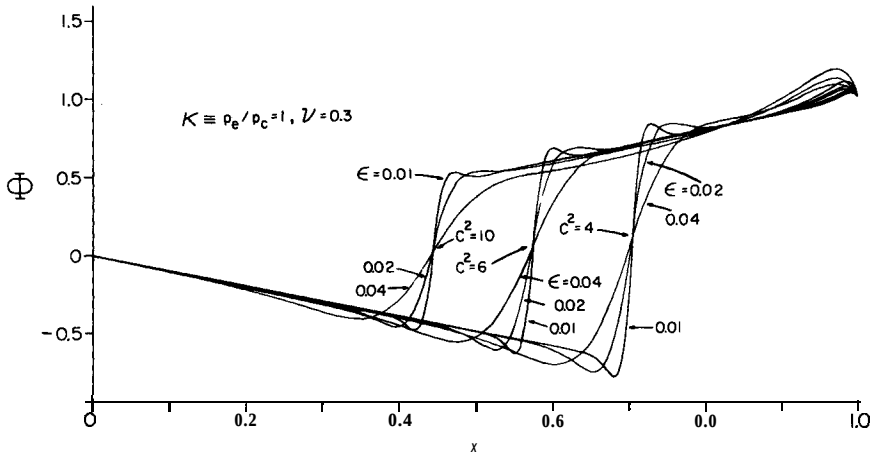

FIG. 2. *Deformed meridional slope profiles for several shallow spherical caps* ($\varepsilon = 0.01, 0.02$ *and 0.04) and load distributions* ($c^2 = 4$, 6, *and* 10) *with peak load level fixed at* p_c ($\kappa = 1$).

points of the solution domain. Based on spline-collocation at Gaussian points with error estimates, the code solves a given problem on a sequence of meshes, automatically increasing the number of mesh points in regions of abrupt changes, until the solution obtained meets a prescribed error tolerance (or until the prescribed maximum mesh is reached without meeting the error tolerance).

In Fig. 2, three sets of numerical solutions for $\Phi(x)$ are given for $\kappa = 1$; they correspond to $c^2 = 4$, 6 and 10, respectively. For each value of c^2, $\Phi(x)$ is given for three thickness parameter values, $\varepsilon = 0.01$, 0.02 and U.04. We see from these plots that, in all cases, the dimple sharpens and the layer width decreases as ε decreases. On the other hand, the actual numerical results show that $\bar{x}_T$, the value of x where the COLSYS solution $\Phi(x)$ vanishes, is well within 2% of the value $\bar{x}_t$. The accuracy in the approximation of x_T by $\bar{x}_t$ improves as ε increases.

In Fig. 3, we show the dimensionless slope $\Phi(x)$ for $\kappa = 1, 10, 30, 50, 100$ and 200 with $\varepsilon = 0.01$ and c = 2. We see from these plots how the sharp dimple deteriorates

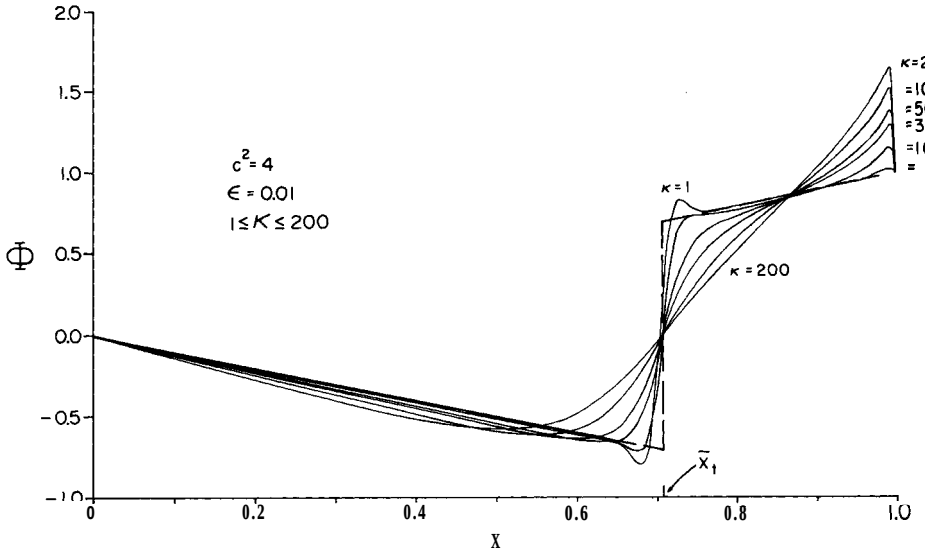

FIG. 3. *Deformed meridional slope profiles of a shallow spherical cap* ($\varepsilon = 0.01$) *with a quadratic pressure distribution* ($c^2 = 4$) *for a range of peak load levels,* $1 \leqq \kappa \leqq 200$.

as κ increases. Nevertheless, the actual numerical results for $\bar{x}_T$ show that the accuracy in the approximation of $\bar{x}_T$ by $\bar{x}_t$ is well within 0.07% for $\kappa = 1$ and improves as κ increases. Fig. 4 shows similar plots of $\Phi(x)$ for $\kappa = 1, 10, 20, 50$, and 100 with $\varepsilon = 0.01$ and $c = \sqrt{10}$. Again the sharp dimple deteriorates as κ increases. Other numerical solutions from COLSYS (see [I] for example) show that the dimple sharpens considerably for the large values of κ if ε is decreased slightly (say by 1/3). In all cases, $\bar{x}_T$ is approximated by $\bar{x}_t$ to within 0.2% and the accuracy improves as κ increases.

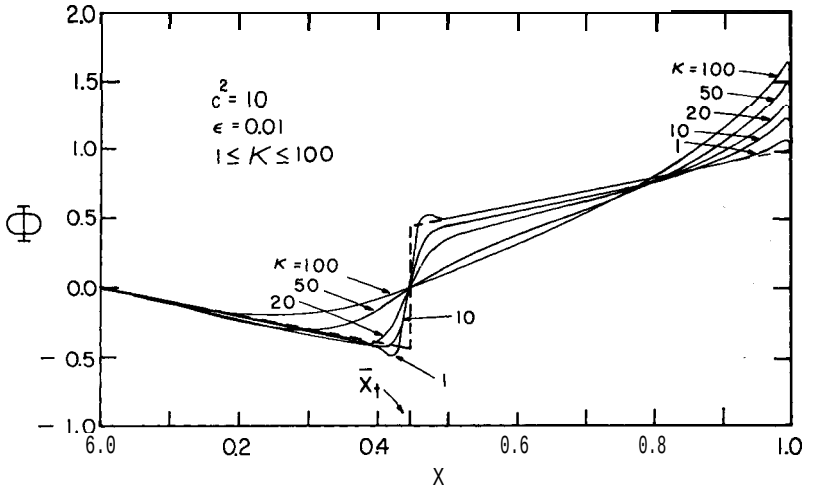

FIG. 4. *Deformed meridional slope profiles of a shallow spherical cap* ($\varepsilon = 0.01$) *with a quadratic pressure distribution* ($c^2 = 10$) *for a range of peak load levels*, $1 \leqq \kappa \leqq 100$.

4. **"Sub-buckling" pressure loading.** When the peak magnitude of the inward pressure loading near the pole is so much smaller than the classical buckling pressure of a spherical shell that p_e/p_c is $O(\varepsilon)$, we have $\kappa = O(\varepsilon)$. For this range of values, we found in § 3 that the leading term inner solution (ϕ_0, ψ_0) is a solution (v, w) to the boundary value problem (3.16) and (3.17) with $v(0) = 0$ suggesting that $v(y)$ and w(y) are respectively odd and even functions. Unlike the situation for larger values of κ, the first integral of the equations which corresponds to (3.14) does not involve $P(x_t)$ and consequently does not provide a condition for the approximate determination of the dimensionless dimple base radius x_T. Therefore, we must investigate higher order terms in the inner expansions for ϕ and ψ. To do this we decompose ϕ and ψ into the forms

$$\phi = v(y) + \varepsilon\bar{\phi}(y, \varepsilon; \kappa), \qquad \psi = w(y) + \varepsilon\bar{\psi}(y, \varepsilon; \kappa), \tag{4.1}$$

where $\bar{\phi} = O(1)$ and $\bar{\psi} = O(1)$ as $\varepsilon \to 0$ for each fixed value of $k \equiv \kappa/\varepsilon$. When we substitute (4.1) into the differential equations (3.6) and (3.7), the leading terms vanish identically because v and w satisfy (3.16) and (3.17). The resulting equations have the form

$$\ddot{\bar{\psi}} + v\bar{\phi} = M(y, \varepsilon; \kappa), \tag{4.2}$$

$$\ddot{\bar{\phi}} - (w\bar{\phi} + v\bar{\psi}) = N(y, \varepsilon; \kappa), \tag{4.3}$$

with

$$M \equiv \frac{1}{x_T}[y(1 - \ddot{\psi}) - \dot{\psi}] + \frac{\varepsilon}{2}\left[\frac{y^2}{x_T^2} + \frac{2\psi}{x_T(x_T + \varepsilon y)} - \bar{\phi}^2\right], \tag{4.4}$$

$$N \equiv \frac{1}{x_T}\left[\frac{4kx}{x_T}P(x) - \dot{\phi} - y\ddot{\phi}\right] + \varepsilon\left[\frac{\phi}{x_T(x_T+\varepsilon y)} + \bar{\phi}\bar{\psi}\right], \tag{4.5}$$

where M and N are O(l) for finite k (and indeed for κ = O(l) with $x_T \sim \bar{x}_t$).

In order to obtain an appropriate condition for the determination of

$$x_t = x_t(k) \equiv \lim_{\varepsilon \to 0} x_T(\varepsilon; k\varepsilon) \qquad (k \text{ fixed}),$$

we do not need to obtain the actual solution for $\bar{\phi}$ and $\bar{\psi}$ (nor, indeed, their leading term asymptotic expressions for small ε). It suffices to work with a first integral of the system (4.2) and (4.3) analogous to the integral in (3.14):

$$\begin{aligned} 0 &= \int_{-\infty}^{y} \{[\ddot{\bar{\psi}} + v\dot{\bar{\phi}} - M]\dot{w} - [\ddot{\bar{\phi}} - w\dot{\bar{\phi}} - v\dot{\bar{\psi}} - N]\dot{v}\}\, dy \\ &= [\dot{\bar{\psi}}\dot{w} - \dot{\bar{\phi}}\dot{v}]_{-\infty}^{y} + \int_{-\infty}^{y} \{-\dot{\bar{\psi}}\ddot{w} + \dot{\bar{\phi}}\ddot{v} + (v\dot{\bar{\phi}} - M)\dot{w} + (w\dot{\bar{\phi}} + v\dot{\bar{\psi}} + N)\dot{v}\}\, dy. \end{aligned} \tag{4.6}$$

We now use *(3.16)* to eliminate $\ddot{v}$ and $\ddot{w}$, giving

$$0 = [\dot{\bar{\psi}}\dot{w} - \dot{\bar{\phi}}\dot{v} - \tfrac{1}{2}\bar{\psi}(1-v^2) + \bar{\phi}vw]_{-\infty}^{y} - \int_{-\infty}^{y} (M\dot{w} - N\dot{v})\, dy. \tag{4.7}$$

In view of the limiting behavior of v and w for large $|y|$ (see (3.17)), we deduce that

$$\int_{-\infty}^{\infty} (M\dot{w} - N\dot{v})\, dy = 0 \tag{4.8}$$

is a necessary condition for the existence of solutions to (4.2) and (4.3) which behave as $y \to \pm\infty$ in such a way that each term in the square brackets in (4.7) vanishes. (That it is also sufficient is a consequence of Fredholm's alternative theorem which may be applied to the **nonself-adjoint** linear operators in (4.2), (4.3) as described in [13, pp. 32-44] and also the Appendix of this paper). Since no approximation has been made in the above derivation, the condition (4.8) determines x_T *exactly*. When $\bar{\phi}$ and $\bar{\psi}$ are approximated to leading order, the unknown parameter x_t is determined, in the same way that the integral relation (3.14) was used to get $x_T \sim \bar{x}_t$ for $\varepsilon \ll_\kappa \ll \varepsilon^{-1}$.

Using the approximations ϕ = v + O(E), ψ = w + $O(\varepsilon)$ in (4.4) and (4.9, we obtain

$$M = x_T^{-1}[y(1-\ddot{w}) - \dot{w}] + O(\varepsilon), \qquad N = x_T^{-1}[4kP(x_T) - \dot{v} - y\ddot{v}] + O(\varepsilon). \tag{4.9}$$

To order ε, the condition (4.8) then is

$$\begin{aligned} 0 &= \frac{1}{x_T}\int_{-00}^{\infty} \{y\dot{w}(1-\ddot{w}) - \dot{w}^2 + \dot{v}^2 + y\dot{v}\ddot{v} - 4k\dot{v}P(x_T)\}\, dy + O(\varepsilon) \\ &= \frac{1}{x_T}[y(w - \tfrac{1}{2}\dot{w}^2 + \tfrac{1}{2}\dot{v}^2) - 4kP(x_T)v]_{-\infty}^{\infty} - \frac{1}{x_T}\int_{-\infty}^{\infty} \left\{W + \tfrac{1}{2}\dot{w}^2 - \tfrac{1}{2}\dot{v}^2\right\} dy + O(\varepsilon). \end{aligned} \tag{4.10}$$

Using (3.16), (3.17) and the first integral $w(1-v^2) = \dot{w}^2 - \dot{v}^2$ (see (3.14)), we deduce the identities

$$\int_{-00}^{\infty} \dot{v}^2\, dy = 3\int_{-\infty}^{\infty} \dot{w}^2\, dy = -\tfrac{3}{5}\int_{-\infty}^{\infty} w\, dy$$

with the (*positive*) value of these three equivalent integrals denoted by I_0 henceforth.

The condition (4.10) now reduces to

$$\frac{8k}{x_T}P(x_T)=\frac{6}{x_T}\int_{-\infty}^{\infty}\dot{w}^2\,dy+O(\varepsilon). \tag{4.11}$$

Recalling that $\kappa=k\varepsilon$ and that our choice of v (y) and $w(y)$ makes the integrand into an even function of y, we may express (4.11) as

$$4\kappa P(x_t)=\varepsilon I_0, \tag{4.12}$$

where the three equivalent expressions for the positive number I_0 may be written as

$$I_0\equiv 6\int_0^{\infty}\dot{w}^2\,dy\;2\int_0^{\infty}\dot{v}^2\,dy=-\tfrac{6}{5}\int_0^{\infty}w\,dy, \tag{4.13}$$

with (v, w) being the ("unique" numerical) solution of (3.16) on $[0,\infty)$. For $\kappa\gg\varepsilon$, the condition (4.12) reduces to (1.2).

The pressure distribution (1.1) gives $P(x)=\frac{1}{4}x(2-c^2x^2)$ so that P vanishes only at $x=0$ and at the two values $x=\pm\bar{x}_t\equiv\pm c^{-1}\sqrt{2}$. For $c>\sqrt{2}$, $P(x)$ is negative in $\bar{x}_t<x<1$ and positive in $0<x<\bar{x}_t$ with maximum value $c^{-1}\sqrt{2/27}$ occurring at (see Fig. 5)

$$x=c^{-1}\sqrt{\tfrac{2}{3}}=\bar{x}_t/\sqrt{3}\equiv x_t^*. \tag{4.14}$$

When $\kappa\gg\varepsilon$, the appropriate solution of (4.12) is $x_t=\bar{x}_t$ as given in (3.15). As $k=\kappa/\varepsilon$ decreases, (4.12) has one positive root which decreases from $\bar{x}_t$ and one which increases from zero until they coalesce at $x=x_t^*$. Therefore, equation (4.12) does not have a (positive) solution when $I_0\varepsilon/4\kappa>P(x_t^*)=c^{-1}\sqrt{\frac{2}{27}}$. The parameter

$$\frac{\kappa_c}{\varepsilon}\equiv k_c=cI_0\sqrt{\tfrac{27}{32}} \tag{4.15}$$

is a critical value for κ/ε; it is an asymptotic estimate of the minimum value of κ/ε for which a finite axisymmetric dimple is possible under the loading (1.1).

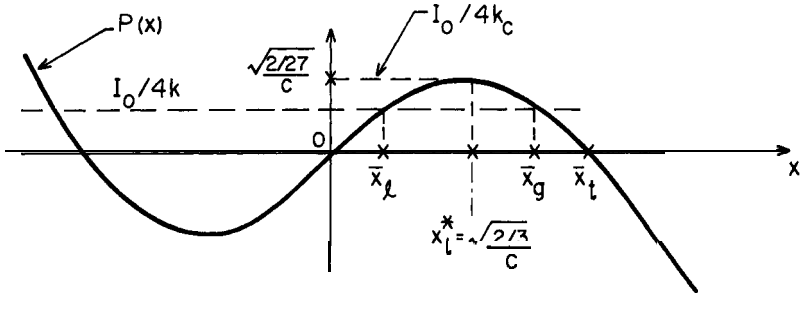

FIG. 5 *Approximate locations of the dimple base for alightly loaded shallow spherical cap.*

As the amplitude $p_e=\kappa p_c$ of the pressure loading (1 .l) increases from zero, the analysis predicts that, to a first approximation, the shell first admits a finite axisymmetric dimple when $\kappa=\varepsilon\kappa_c$, giving

$$p_e=p^*\equiv\varepsilon cI_0p_c\sqrt{\tfrac{27}{32}}.$$

For $\varepsilon c\ll 1$, this value p^* is substantially below the classical buckling pressure for a spherical shell, but nevertheless, the boundary value problem (2.6)–(2.9) allows a

TABLE 1

Exact and asymptotic dimple base radius for $\kappa \equiv p_e/p_c = 1 (\nu = 0.3)$ *(with* $p(x_0) = 0$ *and* $\Phi(\bar{x}_T) = 0$*).*

c^2		4	6	10
$x_0 = 1/c$		0.5	0.408 · · ·	0.316 · · ·
$\bar{x}_t = \sqrt{2}/c$		0.707 · · ·	0.577 · · ·	0.447 · · ·
$\bar{x}_T$	$\varepsilon = 0.01$	0.703	0.574	0.444
	$\varepsilon = 0.02$	0.700	0.571	0.441
	$\varepsilon = 0.04$	0.697 · · ·	0.569 · · ·	0.440 · · ·

finite dimple solution. To a first approximation, the corresponding dimple base radius is $x_t^* = \sqrt{\frac{2}{3}}/c = \bar{x}_t/\sqrt{3}$, so that the pressure acts inwards over the whole of the dimple, decreasing from p_e at the pole to $\frac{1}{3}p_e$ at the dimple base. As κ increases above εk_c, x_t is given by a positive root of (4.12). The smaller root decreases towards zero as κ increases, while the larger increases towards $\bar{x}_t$, giving rise to a smooth change of x_T throughout the range $\varepsilon k_c \lesssim \kappa \ll \varepsilon^{-2}$ (so confirming that $x_T - \bar{x}_t = O(E)$ unless $\kappa = 0$ (1)). To be concrete, we first limit our discussion to the case of the larger positive root; some results for the smaller root will also be discussed later. For the larger positive root, the dimple solution may be represented asymptotically (except for a boundary layer near $x = 1$) by the following leading term of a composite expansion valid throughout the range $\varepsilon k_c \lesssim \kappa \ll \varepsilon^{-1}$:

$$\text{(4.16)} \qquad \begin{aligned} &\Phi \quad (x - x_t) + x_t v(y), \qquad \Psi \sim 4\kappa P(x) + x_t w(y) \qquad (0 \le x \le x_t), \\ &\Phi \sim (x \quad - x_t) + x_t v(y), \qquad \Psi \sim -4\kappa P(x) + x_t w(y) \qquad (x_t \le x \quad < 1), \end{aligned}$$

where $y \equiv (x - x_T)/\varepsilon \sim (x - x_t)/\varepsilon$ with x_t being the larger positive root of (4.12) and where (v, w) is the solution to the boundary value problem (3.16)–(3.17). As κ becomes large compared to ε, then $x_t \to \bar{x}_t$ (with $\bar{x}_t$ taken as 1 if $c \le \sqrt{2}$) and the solution (4.16) approaches the solution (3.27) valid for $\varepsilon \ll \kappa \ll \varepsilon^{-1}$.

The results obtained in this section have been confirmed numerically using COLSYS, both for solution of the original boundary value problem (2.6)–(2.9) for various values of ε, κ and c, and also for evaluating the inner solution v(y), w(y) to (3.16) and (3.17). In this latter calculation, the evaluation of the integral I_0 in (4.13) is carried out concurrently with the solution of (3.16) and (3.17) by solving

$$\dot{J}(y) = -\tfrac{6}{5}w, \qquad J(0) = 0,$$

so that $J(y) \to I_0$ as $y \to \infty$. The solution, to five significant figures of accuracy, was found to be

$$\text{(4.17)} \qquad I_0 = 1.6674 \cdot \cdot \cdot (\simeq \tfrac{5}{3}).$$

The value (4.17) is used in (4.15) to determine the asymptotic estimate $\kappa_c = \varepsilon k_c$ of the lowest load parameter κ for which (finite) polar dimpling is possible under the quadratic load distribution (1 .l). (It may be noted that since k_c is proportional to c, dimpling is not possible when c is as large as ε^{-1} unless p_e is at least comparable with the buckling pressure. This conclusion is not surprising when it is realized that the

pressure acts inward only over $0 \leqq x < c^{-1}$, but acts outward over $c^{-1} < x < 1$ with a magnitude large of order $p_e c^2$ near $x = 1$).

Once k_c and x_t have been computed using (4.12), (4.13) and (4.15), COLSYS may be used to generate numerical solutions of the original boundary value problem (3.6)–(2.9) for a range of values of κ with $k_c \varepsilon \leqq \kappa \ll 1$. The outer solution (3. 1), with x_t chosen (in this discussion) to be the larger positive root $\bar{x}_g$ of (4.12) and $I_0 \simeq 1.6674$, is used as an initial guess for the iterative scheme used in COLSYS. Two sets of COLSYS results for $\Phi(x)$ are presented in Figs. 6 and 7 with $\nu = 0.3$ in all cases and with a relative error tolerance of 10^{-5} or smaller.

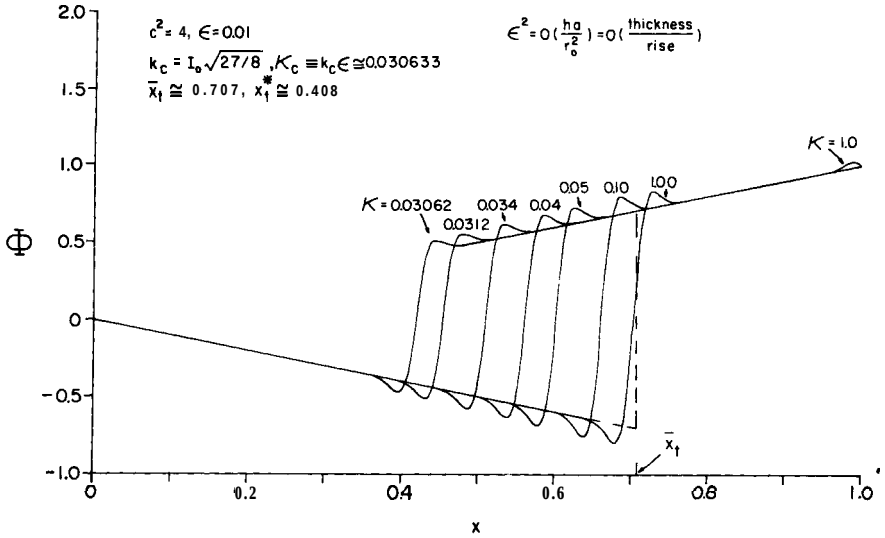

FIG. 6. *Deformed meridional slope profiles of a shallow spherical cap* ($\varepsilon = 0.01$) *under a quadratic pressure distribution* ($c^2 = 4$) *with different peak load levels in the sub-buckling range* ($p_e/p_c \leqq 1.0$).

The curves of $\Phi(x)$, presented in Fig. 6 are for $\varepsilon = 0.01$ and c = 2 for which the quadratic pressure (1 .l) is directed inward over the portion $x < \frac{1}{2}$ of the cap and gives $\bar{x}_t = \frac{1}{2}\sqrt{2} \simeq 0.70711$ and $k_c = I_0(\frac{27}{8})^{1/2} \simeq 3.0633$. Each of the curves corresponds to a different value of κ in the range $O(k_c \varepsilon) \leqq \kappa \leqq 1$. As κ decreases below 1, we see that the dimple base radius generally decreases towards x_t^*. Table 2 shows that $\bar{x}_G$ (the value of x_T from the COLSYS solution with $\bar{x}_g$ as an initial guess) differs from the larger root $\bar{x}_g$ of (4.12) by less than 1% for all $\kappa \geqq \kappa_c$. A dimple solution has been computed for $\kappa = 0.03062$ (which is slightly below $\kappa_c \cong 0.030633$), but not for $\kappa \cong 0.03061$.

Similar results have been obtained for $\varepsilon = 0.02$ and $\varepsilon = 0.04$ as well as for c = $\sqrt{6}$ and $\sqrt{10}$, each for the same three ε values. We only show in Fig. 7 distributions of $\Phi(x)$ for $\kappa = 1.0$, 0.40, 0.25, 0.21, 0.19 and 0.182 in the case of $\varepsilon = 0.04$ and c = $\sqrt{10}$ (with $\kappa_c \cong 0.19374$ and $x_t^* \cong 0.25820$). For this larger value of c, we have a smaller region, $x < 1/\sqrt{10}$, of inward pressure and therewith a smaller $\bar{x}_t$ (~0.44721). Because of the larger ε value (than the one used in Fig. 6), we do not anticipate the same accuracy for $\bar{x}_g$ as an approximation for $\bar{x}_G$. Solutions from COLSYS given in Table 3 in fact show a discrepancy of less than 3% for $\kappa = 1$ to slightly more than 14% for $\kappa = 0.195$. Dimple solutions have been computed for $\kappa = 0.190$ and 0.182 (both below κ_c) with $\bar{x}_G \cong 0.27559$ for the latter which is still above $x_t^* \cong 0.25820$.

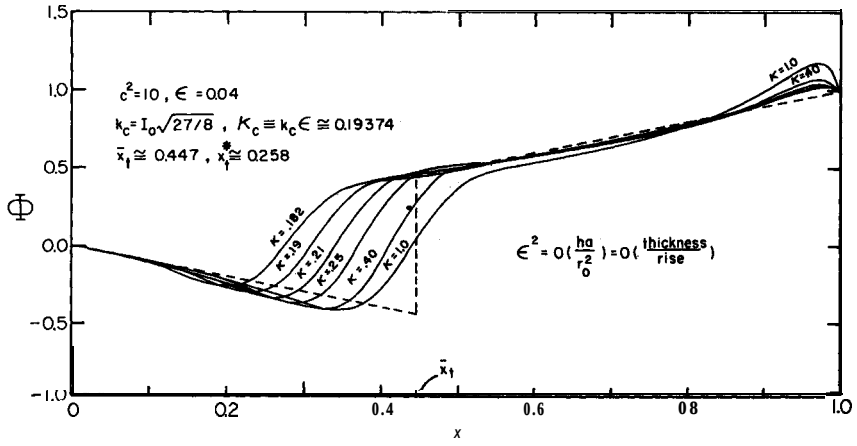

FIG. 7. *Deformed meridional slope profiles of a shallow spherical shell ($\epsilon = 0.04$) under a quadratic pressure load distribution ($c^2 = 10$) with different peak load levels in the sub-buckling range ($p_e/p_c \leqq 1.0$).*

TABLE 2

A comparison between the larger positive root of (1.3), $\bar{x}_g$, and the corresponding COLSYS *solution for $c = 2$ and $\epsilon = 0.01$* ($\bar{x}_t = 0.70711\cdots$, $x_t^* = 0.40825\cdots$, $k_c = 3.0633\cdots$, $\kappa_c = k_c\epsilon$).

κ	$\bar{x}_G$	x_g	κ	$\bar{x}_G$	x_g
10^4	0.70711	0.70711	0.05	0.60169	0.60108
⋯	⋯	⋯	0.04	0.56112	0.56038
20	0.70720	0.70690	0.034	0.51012	0.50908
10	0.70710	0.70669	0.032	0.47901	0.47534
5	0.70670	0.70627	0.031	0.44657	0.44402
1	0.70334	0.70290	0.0307	0.42884	0.42376
0.5	0.69906	0.69862	κ_c	⋯	x_t^*
0.2	0.68572	0.68526	0.03062	0.41984	
0.1	0.66150	0.66101	⋯	⋯	—
0.06	0.62388	0.62333			

* $\bar{x}_G$ is determined by $\Phi(\bar{x}_G) = 0$ where Φ is the COLSYS solution with $\bar{x}_g$ as the initial guess.

TABLE 3

A comparison between the larger positive root of (1.3), $\bar{x}_g$, and the corresponding COLSYS *solution for $c = \sqrt{10}$ and $\epsilon = 0.04$* ($\bar{x}_t = 0.44721\cdots$, $x_t^* = 0.25820\cdots$, $k_c = 4.8436\cdots$, $\kappa_c = k_c\epsilon = 0.19374\cdots$).

κ	$\bar{x}_G$	$\bar{x}_g$	κ	$\bar{x}_G$	$\bar{x}_g$
625	0.44720	0.44719	0.2	0.32856	0.29465
25	0.44705	0.44655	0.195	0.32031	0.27498
⋯			κ_c	⋯	x_t^*
10	0.44683	0.44554	0.190	0.30981	—
5	0.44654	0.44384	⋯	⋯	—
1	0.44165	0.42950	0.182	0.27559	—
0.5	0.42268	0.40914	⋯	⋯	—
0.3	0.39124	0.37515			

* $\bar{x}_G$ is determined by $\Phi(\bar{x}_G) = 0$ where Φ is the COLSYS solution with $\bar{x}_g$ as the initial guess.

It should be noted that a dimple solution corresponding to the smaller positive root of (4.12) is also possible in the sub-buckling pressure load range. We show in Table 4 some results for c 2 and $\varepsilon = 0.04$. For this case, we have $\bar{x}_t \cong 0.70711$, $x_t^* \cong 0.40825$ and $\kappa_c \cong 0.12253$. The COLSYS solutions for x_T for both roots of (4.12) are shown in Table 4. We see from these results that $\bar{x}_g$ is very close to $\bar{x}_G$ except when κ is near κ_c (with a percentage error of less than 11% for $\kappa = 0.1226$) while the smaller root $\bar{x}_l$ is a good approximation for the corresponding COLSYS solution $\bar{x}_L$ (with a percentage error less than 4%) in the limited range $0.13 \leqq \kappa \leqq 0.25$. The discrepancy between $\bar{x}_l$ and $\bar{x}_L$ is about 20% for some κ values near κ_c and near unity given in Table 4.

TABLE 4

A comparison between *the two roots of* (1.3) $0 < \bar{x}_l < \bar{x}_g < \bar{x}_t$, with the corresponding COLSYS solutions *for* $c = 2$ *and* $\varepsilon = 0.04$[1] ($\bar{x}_t = 0.70711$ ..., $x_t^* = 0.40825$ ..., $k_c = 3.0633$ ..., $\kappa_c = k_c\varepsilon = 0.12253$ ...).

κ	$\bar{x}_L$	$\bar{x}_l$	$\bar{x}_G$	x_g
1.00	0.	0.03342	0.69699	0.68980
0.80	0.	0.04183	0.69283	0.68780
0.70	0.04541	0.04786	0.68974	0.68196
0.60	0.06870	0.05593	...	...
0.50	0.08435	0.0673 1	0.67926	0.67105
0.40	0.10002	0.08458	...	...
0.30	0.12297	0.11414		
0.25	0.14303	0.13874	0.63664	0.62746
0.20	0.17830	0.17803	0.61097	0.60108
0.15	0.25 174	0.25580	0.55630	0.54361
0.13	0.31419	0.32550	0.50509	0.48574
0.125	.	...	0.48168	0.45424
0.123	0.35534	0.38798	...	...
0.1226	0.35872	0.40029	0.4655 1	0.41616
κ_c		x_t^*	...	x_t^*
0.1220	0.36424		.	
0.1200	...		0.39107	
0.1196	0.40268		(3)	
...	(2)			

[1] $\bar{x}_G$ and $\bar{x}_L$ are the values of x_T determined by $\Phi(x_T) = 0$ where Φ is the COLSYS solution with $\bar{x}_g$ and $\bar{x}_l$ as the initial guess, respectively.

[2] Could not get COLSYS to converge for $\kappa = 0.1194$ using the solution for $\kappa = 0.1196$ as an initial guess.

[3] Could not get COLSYS to converge for $\kappa = 0.119$ using the solution for $\kappa = 0.120$ as an initial guess.

When Figs. 3 and 6 are compared, it is seen that as κ decreases significantly below 1 the dimple base location begins to differ significantly from the value of $\bar{x}_t$ which the numerical solutions in [1] and [2] had previously indicated as appropriate for $\varepsilon \ll \kappa \ll \varepsilon^{-2}$. The small, but marked, difference $x_T - \bar{x}_t$ which develops in the range $\varepsilon \ll \kappa \ll 1$ significantly increases the amount of computation required for an accurate numerical solution. With the help of the decomposition (4.1), we shall show that $x_T - \bar{x}_t = O(\varepsilon/\kappa)$ throughout $\varepsilon \ll \kappa \ll \varepsilon^{-1}$ and that an appropriate (and more accurate) expression for x_t for all values of $\kappa \ll \varepsilon^{-1}$ is given by a root of

$$4\kappa P(x_t) = \varepsilon I_0, \tag{1.3}$$

(with $I(x_t) = I_0 = J(\infty)$). Such a root may be further expanded for $\mathbf{all}\ \kappa \gg \varepsilon$ as

$$x_t \sim \bar{x}_t + \frac{\varepsilon I_0}{4\kappa P'(\bar{x}_t)} = x_t - \frac{\varepsilon I_0}{4\kappa}, \tag{4.18}$$

where I_0, defined by (4.13), has the positive value (4.17).

Since (4.1) involves no approximations, equations (4.2)–(4.5) still hold exactly, even though $k = \kappa/\varepsilon$ is no longer bounded as $\varepsilon \to 0$. The first term in N may be expanded as

$$\frac{4kx}{x_T^2} P(x) = \frac{4K}{x_T \varepsilon} P(x_T) + \frac{4\kappa}{x_T^2} y[P(x_T) + x_T P'(x_T)] + O(\varepsilon\kappa)$$

so that, correct to O(l), only the two displayed terms contribute to (4.3) and (4.8) when $\kappa \ll 1^{-1}$. Fortunately this changes (4.10) only by the addition of the quantity

$$-\frac{4\kappa}{x_T^2}[P(x_T) + x_T P'(x_T)] \int_{-\infty}^{\infty} y\dot{v}(y)\, dy + O(\varepsilon\kappa).$$

The integrand is an odd function of y, so that the integral vanishes and (4.11) is replaced by

$$4\kappa P(x_T) = \begin{cases} \varepsilon I_0 + O(\varepsilon^2) & (\varepsilon \ll \kappa = O(1)), \\ \varepsilon I_0 + O(\varepsilon^2 \kappa) & (1 \ll \kappa \ll \varepsilon^{-1}). \end{cases}$$

Consequently we obtain

$$4\kappa P(x_T) = \varepsilon I_0 + o(\varepsilon) \tag{4.19}$$

throughout the range $\varepsilon \ll \kappa \ll \varepsilon^{-1}$, and so find that

$$\frac{x_T - \bar{x}_t}{\bar{x}_t} = O(\varepsilon/\kappa), \qquad \varepsilon \ll k \ll \varepsilon^{-1}. \tag{4.20}$$

In particular, by choosing

$$x_T \sim \bar{x}_t \left[1 - \frac{I_0}{4\kappa \bar{x}_t} \varepsilon\right] \tag{4.21}$$

in conjunction with the inextensional bending solution (3.1) as the initial guess for COLSYS for $\varepsilon \ll \kappa =$ O(l) (when $x_T - \bar{x}_t$ is at least as large as the layer width), we can improve the effectiveness and efficiency of the iterative solution scheme by at least an order of magnitude over those with the guess $x_T \sim \bar{x}_t$. Using (4.21), as the initial guess x_t for x_T, the mesh selection and convergence of COLSYS is considerably improved, particularly in the case $\varepsilon = 0.01$ where the transition width is small (Fig. 6). Costly parameter continuation in κ or ε was no longer necessary in nearly all cases investigated.

The above analysis may be modified for a similar improved approximation of x_T for $\varepsilon^2 \ll \kappa^{-1} =$ O(E). However, since $x_T \sim \bar{x}_t$ gives a sufficiently good initial guess for COLSYS in the range indicated, this improved approximation for x_T and its derivation will not be given here. It suffices to note that the analysis and computations of this section and § 3 show that, for a shallow spherical cap subject to the quadratic pressure distribution (1. 1), a transition layer for the dimple solution (3.1) should be expected for $k_c \varepsilon \lesssim \kappa \ll \varepsilon^{-2}$ and that $P(x_T) = 0$ gives a correct leading term approximation to the dimensionless dimple base radius throughout $\varepsilon \ll \kappa \ll \varepsilon^{-2}$. However, a better approximation, valid throughout the range $k_c \varepsilon \lesssim \kappa \ll \varepsilon^{-1}$ is given by a root of (4.12)

since (4.19) holds throughout the range. In the next section, we shall indicate briefly how these results and the corresponding asymptotic solution of the BVP are modified for general dome-shaped shallow shells of revolution subject to a general axisymmetric surface load distribution.

5. Shallow shells of revolution with a normal surface load distribution. The analysis in §§ 3 and 4 is for the boundary value problem (2.6)–(2.9) with $p(x)$ varying quadratically as in (1.1). However, the asymptotic method of solution carries over to the more general boundary value problem (2.1)–(2.7) for a shallow shell of revolution with an undeformed meridional slope $\xi_0\Phi_0(x)$ and a normal load distribution $p_e\hat{p}(x)$ having an axial resultant $-P(x)$ as given by (2.3). We limit ourselves in this paper to a discussion of load distributions and shell shapes for which $xP(x)/\Phi_0(x)$ does not become unbounded in the interval $0 \leqq x \leqq 1$. In particular, we consider only dome-shaped shallow shells of revolution for which the undeformed meridional slope is horizontal only at the pole so that $\Phi_0(x) = 0$ only at $x = 0$ and for which the pole is not a flat point so that $\Phi_0'(0) \neq 0$. (The effects of flat points and points with a horizontal tangent away from the pole on polar dimpling have been investigated in [12] in the range $\kappa \gg \varepsilon$.) For these shallow shells, the leading term outer solution of (2.1)–(2.7) is

$$
\begin{aligned}
&\Phi \sim -\Phi_0(x), \qquad \psi \sim 4\kappa \frac{P(x)}{\Phi_0(x)} \qquad (0 \leqq x < x_T), \\
&\Phi \sim \Phi_0(x), \qquad \psi \sim -4\kappa \frac{P(x)}{\Phi_0(x)} \qquad (x_T < x < 1).
\end{aligned} \tag{5.1}
$$

For $\kappa \gg \varepsilon$, the leading term $\bar{x}_t$ of the dimensionless dimple base radius x_T is still determined by the condition of vanishing axial resultant over the dimpled portion of the shell, $P(\bar{x}_t) = 0$. The determination of the transition layer solution is not greatly changed.

(i) $\kappa\varepsilon \ll 1$. The appropriate choice of the parameters δ and A in (3.3) and (3.4) for this range of κ values for a distinguished limit of (2.1) and (2.2) is now

$$
\delta = \Phi_T \equiv \Phi_0(x_T), \qquad \lambda = \varepsilon\sqrt{x_T/\Phi_T}, \tag{5.2}
$$

so that we have in the transition layer

$$
\Phi(x) = \Phi_T\phi(y), \qquad \Psi = \Phi_T\psi(y), \tag{5.3}
$$

with a stretched variable

$$
y = (x - x_T)/\lambda = (x - x_T)/\varepsilon\sqrt{x_T/\Phi_T}. \tag{5.4}
$$

Equation (5.4) shows that the stretching (and therefore the transition layer width) in general depends on the load distribution (through x_T), the shell shape (through $\Phi_T \equiv \Phi_0(x_T)$) as well as the shell thickness parameter ε. Only in the case of a spherical cap ($\Phi_0(x) = x$) do the effects of shell shape and loading cancel out leaving $y = (x - x_T)/\varepsilon$ so that the transition layer width is controlled by the thickness parameter alone. Numerical results supporting this observation can be found in [12] (see also [21]).

In view of (5.2)–(5.4), the leading term inner (or transition layer) solution may be written for all $\kappa \ll \varepsilon^{-1}$ as $\phi_0 = v(y), \psi_0 = w(y)$, where v(y) and $w(y)$ are as defined by (3.16) and (3.17), but the stretched variable y is now given by (5.4). The location of the dimple base is determined by methods closely analogous to those of § 4, with

the quantities M and N amended as

$$M = \frac{-1}{\sqrt{x_T \Phi_T}}[y\ddot{\psi} + \dot{\psi}] + \frac{1}{2\varepsilon \Phi_T^2}[\Phi_0^2(x) - \Phi_T^2] + \frac{\varepsilon}{2}\left(\frac{2\psi}{x\Phi_T} - \bar{\phi}^2\right)$$

$$= \frac{1}{\sqrt{x_T \Phi_T}}\left[y\frac{x_T}{\Phi_T}\Phi_0'(x_T) - y\ddot{\psi} - \dot{\psi}\right] + O(\varepsilon), \tag{5.5}$$

$$N = \frac{1}{\sqrt{x_T \Phi_T}}\left[\left(\frac{x_T}{\Phi_T}\right)^{3/2}\frac{4kx}{x_T}P(x) - \dot{\phi} - y\ddot{\phi}\right] + \varepsilon\left[\frac{\phi}{x\Phi_T} + \frac{xQ(x)}{\Phi_T^2} + \bar{\phi}\bar{\psi}\right],$$

and with Φ_T and A defined by (5.2) and x $= x_T + \lambda y$. The resulting integrated condition (4.8) shows that the limiting value

$$x_t = x_t(k) = \lim_{\varepsilon \to 0} x_T(\varepsilon, k\varepsilon)$$

satisfies the equation

$$4\kappa P(x_t) = \varepsilon I(x_t), \tag{1 | 3}$$

where

$$I(x_t) = \left(\frac{\Phi_t}{x_t}\right)^{3/2}\left[\frac{1}{3} + \frac{5}{3}\frac{x_t}{\Phi_t}\Phi_0'(x_t)\right]\int_0^\infty v^2\,dy = \frac{1}{6}I_0\left[\frac{\Phi_t}{x_t}\right]^{1/2}\frac{\Phi_t + 5x_t\Phi_0'(x_t)}{x_t} \tag{5.6}$$

and where $\Phi_t = \Phi_0(x_t)$.

The condition (1.3) for the determination of x_t has a right-hand side which is no longer a pure number; it depends on the unknown parameter x_t through the undeformed shape function Φ_0(x), as given in (5.6). The resulting equation is somewhat more complicated than in the special case of the spherical cap, for which $I(x_t)$ reduces to the constant value $I_0 =$ 1.6674 .. computed using COLSYS, but may readily be solved either numerically or graphically. Rearranging (1.3) and (5.6) as

$$k = \frac{\kappa}{\varepsilon} = \frac{I(x_t)}{4P(x_t)} = I_0\left[\frac{\Phi_0(x_t)}{x_t}\right]^{1/2}\frac{\Phi_0(x_t) + 5x_t\Phi_0'(x_t)}{24x_tP(x_t)} \tag{5.7}$$

we see that once $\Phi_0(x)$ and $P(x)$ are specified, the function $4P(x)/I(x)$ is easily constructed from $\Phi_0(x)$ and I_0 and the approximate dimple base radius $x_t(k)$ may then be determined from (5.7), by numerical methods if necessary. In particular, we see that the minimum value k_c of $k \equiv \kappa/\varepsilon$ is given by the minimum value in $0 < x < 1$ of $I(x)/4P(x)$. This corresponds to the maximum of $4P(x)/I(x)$ and determines the limiting base radius x_t^*. As for the spherical cap, we see that one solution of (5.7) has $x_t(k) \to \bar{x}_t$, where $P(\bar{x}_t) = 0$, as κ increases. Again we have $x_T \sim \bar{x}_t$ for $\kappa \gg \varepsilon$ with $x_T - \bar{x}_t = O(\varepsilon)$ and $x_T - x_t = O(\varepsilon^2)$ for $\varepsilon \ll \kappa \ll \varepsilon^{-1}$.

(ii) $1 \ll \kappa = O(\varepsilon^{-1})$. When κ increases to become comparable with ε^{-1}, an extra term survives in the limit equations, However, we again obtain $\phi \sim V(y;\beta), \psi \sim W(y;\beta)$, where

$$\beta = -\frac{4\kappa\varepsilon}{\bar{x}_t}\left(\frac{\bar{x}_t}{\Phi_t}\right)^{5/2}P'(\bar{x}_t), \quad y = \left(\frac{\Phi_T}{x_T}\right)^{1/2}\frac{x - x_T}{\varepsilon}, \quad x_T - \bar{x}_t = O(\varepsilon^2), \tag{5.8}$$

with the odd function V and the even function W determined by the system (3.20) and (3.21).

As in the case of quadratic pressure loadings on a spherical shell, for which $4P(x)/I(x)$ increases from zero to a maximum and eventually becomes negative, we

anticipate that for some choices of $\Phi_0(x)$ and $p(x)$ equation (5.7) will have more than one solution. Since numerical integration of (2.5)–(2.9) yields values $\bar{x}_L$ corresponding to ranges in which $P(x)$ is increasing, we anticipate that dimpling is possible in the "sub-buckling" range for a *uniform pressure distribution*:

$$p = p_e \quad \text{in } 0 \leqq x < 1, \qquad \text{giving } P(x) = \tfrac{1}{2}x.$$

Similarly, dimpling should occur for shells with *localized uniform external pressure* over a circular region centered at the apex:

$$p = \begin{cases} p_e, & 0 \leqq x < x_1 \\ 0, & x_1 < x < 1 \end{cases}, \quad \text{giving} \quad P(x) = \begin{cases} \dfrac{x}{2}, & 0 \leqq x < x_1, \\ \dfrac{x_1^2}{2x}, & x_1 < x < 1, \end{cases}$$

even though in neither case is there a solution to $P(x) = 0$, $x \neq 0$. Also, the possibility of "inverted dimples" exists, near roots of $4\kappa P(x) = -\varepsilon I(x)$, since transition from $\Phi \sim \Phi_0(x)$ $(x < x_T)$ to $\Phi \sim -\Phi_0(x)$ $(x > x_T)$ has leading term inner solution given by $\Phi \sim -\Phi_T v(y)$ which will alter (4.10) and (1.3) only by changes of sign.

(iii) $1 \ll \kappa\varepsilon \ll \varepsilon^{-1}$. Further increase of $\bar{\kappa} \equiv \kappa\varepsilon \gg 1$, causes a widening of the transition layer. It leads to the choice of scaling

$$\lambda = \kappa\varepsilon^2\left(\frac{x_T}{\Phi_T}\right)^3, \qquad \delta = \kappa^2\varepsilon^2 x_T\left(\frac{x_T}{\Phi_T}\right)^4 \tag{5.9}$$

such that $\Phi \sim \Phi_T \bar{V}(y)$, $\Psi \sim \delta \bar{W}(y)$, where the functions $\bar{V}(y)$ and $\bar{W}(y)$ satisfy the equations (3.22) and (3.23) with γ again given by $\gamma = -4\bar{x}_t^{-1}P'(\bar{x}_t)$. The only changes from § 3 are the extra powers of x_T/Φ_T, since we still have

$$x - x_T = \lambda y, \qquad x_T = \bar{x}_t + o(\lambda).$$

For still larger values of κ, so that $(\kappa\varepsilon^2)^{-1} = O(1)$ at most, no transition layer can be expected as nonlinear membrane action dominates throughout the cap except near the edges (see [17]).

From the above observations we deduce that the results derived in §§ 3 and 4 for spherical caps subjected to a quadratic pressure loading are easily extended to describe more general caps under general axisymmetric pressure loading.

6. Conclusions. We have shown by an asymptotic analysis how, for a wide range of axisymmetric shapes of elastic caps subjected to a general class of axisymmetric pressure loadings, dimpled configurations may occur for a wide range of values of a thickness parameter ε and a loading parameter κ. Previous results for spherical caps [1], [2] are thereby greatly extended; significant new features of the phenomena are also delineated.

The asymptotic analysis, based on a small thickness parameter ε, predicts that a good approximation x_t to the base radius of possible dimpled configurations is given by the single equation

$$4\kappa P(x_t) = \varepsilon I(x_t) \tag{1.3}$$

throughout the parameter range $\kappa\varepsilon = O(1)$, $\varepsilon \ll 1$, with $I(x_t)$ given in terms of $\Phi_0(x)$ and I_0 by the simple relation (5.6). Although this reduces to the simpler criterion $P(\bar{x}_t) = 0$ (see [1], [17]) for loadings $\kappa^{-1} = O(1)$, it predicts also that dimpled states may occur for pressure loadings $\kappa = o(1)$, below the classical buckling pressure of a spherical shell, a fact not previously known even for a spherical cap under the quadratic

pressure distribution (1 .l). Moreover, a root x_t of (1.3) as an initial guess for the dimensionless dimple radius leads to much more rapid convergence of iterative numerical solution schemes than the corresponding root $\bar{x}_t$ of $P(\bar{x}_t)=0$ even for $\kappa \gg \varepsilon$. The predictions of (1.3) are verified by numerical solutions of the full system of equations and also prove invaluable for efficient mesh selection in that numerical calculation, as described in § 4.

We do not claim here that a dome-shaped cap will dimple when the loading magnitude is first raised into the relevant parameter range. We predict merely that the dimpled state is one possible configuration. It seems reasonable to conjecture that a cap, once dimpled at high loading might remain dimpled as the loading is reduced below the classical buckling pressure. Also the analysis allows the possibility of more than one dimpled state corresponding to the same loading, and this prediction is confirmed numerically by COLSYS. These results will be unified by an overall load-deflection relation of the type obtained in [16] (the &norm of $(\Phi-\Phi_0)$ vs. κ) generated for spherical caps in [15].

The importance of interpreting the results of the present paper in the light of a relevant overall load-deformation relation can be seen more conspicuously from the case of a spherical cap under a uniform external pressure distribution. For that case, we have $P(x)=x/2$ and the condition (1.3) becomes

$$2\kappa x_t = \varepsilon I_0 \tag{6.1}$$

or $x_t = \varepsilon I_0/2\kappa$. In other words, the size of the dimple increases as the magnitude of the uniform pressure distribution tends to zero! It will be seen from the results of [15] that the load-dimple size relation (6.1) applies for $\kappa/\varepsilon \gg \varepsilon$; for smaller κ values, $\kappa = O(\varepsilon^2)$, the deformation pattern is no longer a polar dimpling pattern. Mathematically, for $\kappa \ll \varepsilon$, the scaling used in the present paper is no longer appropriate and the problem should be analyzed again after re-scaling.

Appendix. The **"alternative"** method. The differences $\phi - \mathrm{v} = \varepsilon\bar{\phi}(y), \psi - w = \varepsilon\bar{\psi}(y)$ between the exact functions (ϕ, ψ) and their leading order approximations (v (y), w(y)) within the transition layer satisfy equations of the form

$$\ddot{\bar{\psi}} + v(y)\bar{\phi} = M(y;\varepsilon,\kappa), \qquad \ddot{\bar{\phi}} - w(y)\bar{\phi} - v(y)\bar{\psi} = N(y;\varepsilon,\kappa), \tag{A.1}$$

where y $= (x - x_T)/\lambda$ and M, N are given by (4.4), (4.5), or the generalization (5.5) for caps of general undeformed shape $\Phi_0(x)$. Additionally the behavior of $(\bar{\phi}, \bar{\psi})$ as $y \to \pm\infty$ is determined by matching to the outer solutions valid on either side of the dimple base. We now show that (4.8) is the necessary ***and sufficient*** condition for such quantities $(\bar{\phi}, \bar{\psi})$ to exist.

First let $f(y)$ and g(y) be any twice differentiable functions having the behavior required of $\bar{\phi}(y)$ and $\bar{\psi}(y)$ respectively as y $\to \pm\infty$. Then write

$$\bar{\phi}(y) = \phi^*(y) + f(y), \qquad \bar{\psi}(y) = \psi^*(y) + g(y) \tag{A.2}$$

so that $\phi^*(y)$ and $\psi^*(y)$ satisfy the system of linear equations

$$\ddot{\psi}^* + v(y)\phi^* = M^*(y), \qquad \ddot{\phi}^* - w(y)\phi^* - v(y)\psi^* = N^*(y), \tag{A.3}$$

subject to the homogeneous conditions

$$y \to \pm\infty: \quad \phi^*(y) \to 0, \quad \psi^*(y) \to 0 \tag{A.4}$$

where

$$M^* \equiv M - \ddot{g} - vf, \qquad N^* \equiv N - \ddot{f} + wf + vg, \tag{A.5}$$

anticipate that for some choices of $\Phi_0(x)$ and p(X) equation (5.7) will have more than one solution. Since numerical integration of (2.5)–(2.9) yields values $\bar{x}_L$ corresponding to ranges in which $P(x)$ is increasing, we anticipate that dimpling is possible in the "sub-buckling" range for a *uniform pressure distribution*:

$$p = p_e \quad \text{in } 0 \leqq x < 1, \qquad \text{giving } P(x) = \tfrac{1}{2}x.$$

Similarly, dimpling should occur for shells with ***localized uniform external pressure*** over a circular region centered at the apex:

$$p = \begin{cases} p_e, & 0 \leqq x < x_1 \\ 0, & x_1 < x < 1 \end{cases}, \quad \text{giving} \quad P(x) = \begin{cases} \dfrac{x}{2}, & 0 \leqq x < x_1, \\ \dfrac{x_1^2}{2x}, & x_1 < x < 1, \end{cases}$$

even though in neither case is there a solution to $P(x) = 0, x \neq 0$. Also, the possibility of "inverted dimples" exists, near roots of $4\kappa P(x) = -\varepsilon I(x)$, since transition from $\Phi \sim \Phi_0(x)\,(x < x_T)$ to CD- --@"(x) $(x > x_T)$ has leading term inner solution given by $\Phi \sim -\Phi_T v$ (y) which will alter (4.10) and (1.3) only by changes of sign.

(iii) $1 \ll \kappa\varepsilon \ll {}_{\iota}{}^{-1}$. Further increase of $\bar{\kappa} \equiv \kappa\varepsilon \gg 1$, causes a widening of the transition layer. It leads to the choice of scaling

$$\lambda = \kappa\varepsilon^2 \left(\frac{x_T}{\Phi_T}\right)^3, \qquad \delta = \kappa^2\varepsilon^2 x_T \left(\frac{x_T}{\Phi_T}\right)^4 \tag{5.9}$$

such that $\Phi \sim \Phi_T \bar{V}(y), \Psi \sim \delta \bar{W}(y)$, where the functions $\bar{V}(y)$ and $\bar{W}(y)$ satisfy the equations (3.22) and (3.23) with γ again given by $\gamma = -4\bar{x}_t^{-1} P'(\bar{x}_t)$. The only changes from § 3 are the extra powers of x_T/Φ_T, since we still have

$$x - x_T = \lambda y, \qquad x_T = \bar{x}_t + o(\lambda).$$

For still larger values of κ, so that $(\kappa\varepsilon^2)^{-1} = 0(1)$ at most, no transition layer can be expected as nonlinear membrane action dominates throughout the cap except near the edges (see [17]).

From the above observations we deduce that the results derived in §§ 3 and 4 for spherical caps subjected to a quadratic pressure loading are easily extended to describe more general caps under general axisymmetric pressure loading.

6. **Conclusions.** We have shown by an asymptotic analysis how, for a wide range of axisymmetric shapes of elastic caps subjected to a general class of axisymmetric pressure loadings, dimpled configurations may occur for a wide range of values of a thickness parameter ε and a loading parameter κ. Previous results for spherical caps [1], [2] are thereby greatly extended; significant new features of the phenomena are also delineated.

The asymptotic analysis, based on a small thickness parameter ε, predicts that a good approximation x_t to the base radius of possible dimpled configurations is given by the single equation

$$4\kappa P(x_t) = \varepsilon I(x_t) \tag{1.3}$$

throughout the parameter range $\kappa\varepsilon = \mathbf{O(1)}$, $\varepsilon \ll 1$, with $I(x_t)$ given in terms of $\Phi_0(x)$ and I_0 by the simple relation (5.6). Although this reduces to the simpler criterion $P(\bar{x}_t) = 0$ *(see* [1], [17]) for loadings $\kappa^{-1} = \mathrm{O(1)}$, it predicts also that dimpled states may occur for pressure loadings $\kappa = o$ (1), below the classical buckling pressure of a spherical shell, a fact not previously known even for a spherical cap under the quadratic

pressure distribution (1 .l). Moreover, a root x_t of (1.3) as an initial guess for the dimensionless dimple radius leads to much more rapid convergence of iterative numerical solution schemes than the corresponding root $\bar{x}_t$ of $P(\bar{x}_t)=0$ even for $\kappa \gg \varepsilon$. The predictions of (1.3) are verified by numerical solutions of the full system of equations and also prove invaluable for efficient mesh selection in that numerical calculation, as described in § 4.

We do not claim here that a dome-shaped cap will dimple when the loading magnitude is first raised into the relevant parameter range. We predict merely that the dimpled state is one possible configuration. It seems reasonable to conjecture that a cap, once dimpled at high loading might remain dimpled as the loading is reduced below the classical buckling pressure. Also the analysis allows the possibility of more than one dimpled state corresponding to the same loading, and this prediction is confirmed numerically by COLSYS. These results will be unified by an overall load-deflection relation of the type obtained in [16] (the l_2-norm of $(\Phi-\Phi_0)$ vs. κ) generated for spherical caps in [15].

The importance of interpreting the results of the present paper in the light of a relevant overall load-deformation relation can be seen more conspicuously from the case of a spherical cap under a uniform external pressure distribution. For that case, we have $P(x)=x/2$ and the condition (1.3) becomes

$$2\kappa x_t = \varepsilon I_0 \tag{6.1}$$

or $x_t=\varepsilon I_0/2\kappa$. In other words, the size of the dimple increases as the magnitude of the uniform pressure distribution tends to zero! It will be seen from the results of [15] that the load-dimple size relation (6.1) applies for $\kappa/\varepsilon \gg \varepsilon$; for smaller κ values, $\kappa=O(\varepsilon^2)$, the deformation pattern is no longer a polar dimpling pattern. Mathematically, for $\kappa \ll \varepsilon$, the scaling used in the present paper is no longer appropriate and the problem should be analyzed again after re-scaling.

Appendix. The "alternative" method. The differences $\phi-v=\varepsilon\bar{\phi}(y), \psi-w=\varepsilon\bar{\psi}(y)$ between the exact functions (ϕ,ψ) and their leading order approximations (v(y), $w(y)$) within the transition layer satisfy equations of the form

$$\ddot{\bar{\psi}}+v(y)\bar{\phi}=M(y;\varepsilon,\kappa), \qquad \ddot{\bar{\phi}}-w(y)\bar{\phi}-v(y)\bar{\psi}=N(y;\varepsilon,\kappa), \tag{A.1}$$

where y $=(x-x_T)/\lambda$ and M, N are given by (4.4), (4.9, or the generalization (5.5) for caps of general undeformed shape $\Phi_0(x)$. Additionally the behavior of $(\bar{\phi},\bar{\psi})$ as $y\to\pm\infty$ is determined by matching to the outer solutions valid on either side of the dimple base. We now show that (4.8) is the necessary *and sufficient* condition for such quantities $(\bar{\phi},\bar{\psi})$ to exist.

First let $f(y)$ and g(y) be any twice differentiable functions having the behavior required of $\bar{\phi}(y)$ and $\bar{\psi}(y)$ respectively as y $\to\pm\infty$. Then write

$$\bar{\phi}(y)=\phi^*(y)+f(y), \qquad \bar{\psi}(y)=\psi^*(y)+g(y) \tag{A.2}$$

so that $\phi^*(y)$ and $\psi^*(y)$ satisfy the system of linear equations

$$\ddot{\psi}^*+v(y)\phi^*=M^*(y), \qquad \ddot{\phi}^*-w(y)\phi^*-v(y)\psi^*=N^*(y), \tag{A.3}$$

subject to the homogeneous conditions

$$y\to\pm\infty: \quad \phi^*(y)\to 0, \quad \psi^*(y)\to 0 \tag{A.4}$$

where

$$M^*\equiv M-\ddot{g}-vf, \qquad N^*\equiv N-\ddot{f}+wf+vg, \tag{A.5}$$

dots denote derivatives with respect to y and we have suppressed the dependence on I and κ. Systems of the type (A.3), (A.4) occur frequently in singular perturbation problems and have the form

$$\mathbf{L}\mathbf{u} = \mathbf{M}(y), \qquad y \in (a, b), \tag{A.6}$$

where L is a linear differential operator, u is the vector of unknowns, M is a vector function which is known in principle (to within a number of parameters at any stage in the perturbation or iteration process) and u satisfies homogeneous boundary conditions at y = a and y = b. When the operator L*, adjoint to L, possesses a nontrivial null-space corresponding to the given boundary conditions, the system (A.6) possesses solutions if and only if M(y) is orthogonal to all elements of this null-space. This criterion usually provides just sufficient conditions to determine the "free" parameters-for example, those which arise in the perturbation expansions for the frequency and amplitude of a nonlinear oscillation [10], [14]. The general procedure is known as the *Fredholm alternative*, for which results appropriate to the system (A.3) and (A.4) may be found in [13].

The linear system (A.3), (A.4) may be written in matrix form as

$$\begin{aligned} &\dot{\mathbf{u}}(y) - \mathbf{A}(y)\mathbf{u}(y) = \mathbf{M} \qquad (-\infty < y < \infty) \\ &y \to \pm\infty: \quad \mathbf{u} \to \mathbf{0} \end{aligned} \tag{A.7}$$

where

$$\mathbf{u} \equiv \begin{pmatrix} \phi^* \\ \psi^* \\ \dot{\phi}^* \\ \dot{\psi}^* \end{pmatrix}, \quad \mathbf{A} \equiv \begin{bmatrix} 0 & 0 & 1 & 0 \\ 0 & 0 & 0 & 1 \\ w(y) & v(y) & 0 & 0 \\ -v(y) & 0 & 0 & 0 \end{bmatrix}, \quad \mathbf{M} \equiv \begin{pmatrix} 0 \\ 0 \\ N^* \\ M^* \end{pmatrix}.$$

The adjoint homogeneous problem is

$$\begin{aligned} &\dot{\mathbf{v}}(y) + \mathbf{A}^T(y)\mathbf{v}(y) = 0 \qquad (-\infty < y < \infty), \\ &y \to \pm\infty: \quad \mathbf{v} \to \mathbf{0} \end{aligned}$$

which is equivalent to

$$\begin{aligned} &\ddot{s}(y) + v(y)r(y) = 0, \qquad \ddot{r}(y) - w(y)r(y) - v(y)s(y) = 0, \\ &y \to \pm\infty: \quad r \to 0, \quad s \to 0, \end{aligned} \tag{A.8}$$

when we write v = [i(y), $-\dot{s}(y), -r(y), s(y)]^T$ and T denotes a transpose. Since differentiation of (3.16) gives

$$\ddot{w}(y) + v(y)\dot{v}(y) = 0, \qquad \ddot{v}(y) - w(y)\dot{v}(y) - v(y)\dot{w}(y) = 0,$$

it can be seen that

$$r = \dot{v}(y), \qquad s = \dot{w}(y), \tag{A.9}$$

is one solution to (A.8). Actually, all solutions to (A.8) are derivable from v(y) and $w(y)$.

Suppose that the problem (3.16), (3.17) has a family of solutions {v (y; α), w (y; α)} which are continuously differentiable with respect to the parameter α, with $v(y ; 0)$ = v (y), w (y ; 0) = w (y). Then, using the subscript α to denote a partial derivative, we have

$$\frac{d^2 w_\alpha}{dy^2} + v(y;\alpha) v_\alpha = 0, \qquad \frac{d^2 v_\alpha}{dy^2} - w(y;\alpha) v_\alpha - v(y;\alpha) w_\alpha = 0,$$

$$y \to \pm\infty: \quad v_\alpha \to 0, \quad w_\alpha \to 0.$$

Setting $\alpha = 0$, we see that each solution (r, s) to (A.8) is an infinitesimal generator of the group of solutions to (3.16) and (3.17). Under our previous assumption that all such solutions may be parametrized as $\{v(y + C), w(y + C)\}$, we set $C = \alpha$ and obtain

$$v_\alpha(y;0) = \dot{v}(y), \qquad w_\alpha(y;0) = \dot{w}(y).$$

Hence the null-space defined by the homogeneous problem (A.8) is spanned by the single basis element $\mathbf{v} = [\ddot{v}(y), -\ddot{w}(y), -\dot{v}(y), \dot{w}(y)]^T$. Fredholm's alternative theorem for the nonself-adjoint case (see Cesari [13] pp. 32-34) then states that (A.7) possesses a solution *if and only if*

$$0 = \int_{-\infty}^{\infty} \mathbf{v}^T \cdot \mathbf{M}\, dy = \int_{-\infty}^{\infty} (-\dot{v}N^* + \dot{w}M^*)\, dy.$$

Using (A.5), integration by parts and the differential equations (3.16) we then obtain

$$\begin{aligned}
\int_{-\infty}^{\infty} (M\dot{w} - N\dot{v})\, dy &= \int_{-\infty}^{\infty} (\ddot{g}\dot{w} + vf\dot{w} - \ddot{f}\dot{v} + wf\dot{v} + vg\dot{v})\, dy \\
&= [\dot{g}\dot{w} - \dot{f}\dot{v}]_{-\infty}^{\infty} + \int_{-\infty}^{\infty} [\dot{f}\ddot{v} - \dot{g}\ddot{w} + f(v\dot{w} + w\dot{v}) + gv\dot{v}]\, dy \\
&= [\dot{g}\dot{w} - \dot{f}\dot{v}]_{-\infty}^{\infty} + \int_{-\infty}^{\infty} [\dot{f}vw - \tfrac{1}{2}\dot{g}(1 - v^2) + f(v\dot{w} + w\dot{v}) + gv\dot{v}]\, dy \\
&= [\dot{g}\dot{w} - \dot{f}\dot{v} + fvw - \tfrac{1}{2}g(1 - v^2)]_{-\infty}^{\infty}.
\end{aligned}$$

Since it can be shown that $v \to \pm 1$ and $w \to 0$ exponentially as $y \to \pm\infty$, whilst the matching requires only that f and g behave algebraically, we deduce the required restriction

$$\int_{-\infty}^{\infty} (M\dot{w} - N\dot{v})\, dy = 0. \tag{4.8}$$

Acknowledgments. This research is partly supported by NSERC Operating Grants A9259 and A9117 and, in the case of the second author, also by a U.B.C. Killam Senior Fellowship. The authors would like to thank Messrs. Eric Kong and Keith Anderson for assistance with the computing and machine plots and Professors C. Lange and H. J. Weinitschke for their helpful comments.

REFERENCES

[1] F. Y. M. Wan, *The dimpling of spherical cups,* Mechanics Today (The Eric Reissner Anniversary Volume), 5 (1980), pp. 495–508.

[2] ——— *Polar dimpling of complete spherical shells,* Theory of Shells, Proc. Third IUTAM Shell Symposium, Tbilisi, USSR, August, 1978, W. T. Koiter and G. K. Mikhailov, eds., North-Holland, Amsterdam, 1980, pp. 191-207.

[3] C. V. Ranjan and C. R. Steele, *Large deflection of deep spherical shells under concentrated load,* Tech. Paper No. 77-411, AIAA/ASME 18th Structures, Structural Dynamics and Materials Conference, San Diego, March 1977, also Proc. of same conference, pp. 269-278.

[4] D. G. ASHWELL, *On the large deflexion of a spherical shell with an inward point load,* Proc. First Symposium on Thin Elastic Shells, Delft, the Netherlands, August, 1959, W. T. Koiter, ed., North-Holland, Amsterdam, 1960, pp. 43-63.

[5] U. ASCHER, J. CHRISTIANSEN AND R. D. RUSSELL, *A collocation solver for mixed order systems of boundary value problems,* Math. Comp., 33 (1979), pp. 659-679.

[6] E. REISSNER, *On axisymmetric deformations of thin shells of revolution,* Proc. Symposia in Appl. Math., III, American Mathematical Society, Providence, RI, 1950, pp. 27-52.

[7] ———, *Symmetric bending of shallow shells of revolution,* J. Math. Mech., 7 (1958), pp. 121–140.

[8] ———, *The edge effect in symmetric bending of shallow shells of revolution,* Comm. Pure Appl. Math., 12 (1959), pp. 385-398.

[9] J. D. COLE, *Perturbation Methods in Applied Mathematics,* Ginn Blaisdell, Waltham, MA, 1968. (Also J. Kevorkian and J. D. Cole, Springer-Verlag, New York-Heidelberg-Berlin, 1981.)

[10] A. NAYFEH, *Perturbation Methods,* Academic Press, New York, 1973.

[11] P. C. FIFE, *Transition layers in singular perturbation problems,* J. Differential Equations, 15 (1974), pp. 77–105.

[12] F. Y. M. WAN AND U. ASCHER, *Horizontal and flat points in shallow shell dimpling,* IAMS Tech. Report No. 80-5, Univ. British Columbia, May 1980, Proc. of BAIL I Conference, Dublin, 1980, J. Miller, ed., Boole Press, Dublin, 1980, pp. 415-419.

[13] L. CESARI, *Nonlinear Functional Analysis and Differential Equations,* Marcel Dekker, New York, 1976.

[14] N. N. BOGOLIUBOV AND Y. A. MITROPOLSKY, *Asymptotic Methods in the Theory of Nonlinear Oscillations,* Hindustan, New Delhi, 196 1.

[15] c. G. LANGE AND F. Y. M. WAN, *Bifurcation analysis of spherical shells,* IAMS Tech. Rep. 83-22, Univ. British Columbia, Vancouver, Oct., 1983.

[16] L. BAUER, E. L. REISS AND H. B. KELLER, *Axisymmetric buckling of hollow spheres and hemispheres,* Comm. Pure Appl. Math., 23 (1970), pp. 529-568.

[17] F. Y. M. WAN, *Shallow caps with a localized pressure distribution centered at the apex,* IAMS Tech. Report No. 79-44, Univ. British Columbia, Vancouver, August 1979, also Proc. EUROMECH Colloquium (# 165) on Flexible Shells (Munich, 1983), E. Axelrod and F. Emmerling, eds., Springer-Verlag, Berlin, to appear.

[18] L. L. BUCCIARELLI, *The analysis of propellant expulsion bladders and diaphrams,* Dept. of Aero. & Astro. Tech. Report, Massachusetts Institute of Technology, Cambridge, 1967.

[19] W. W. FENG AND W. H. YANG, *On the contact problem of an inflated spherical membrane,* J. Appl. Mech., 40 (1973), pp. 209–214.

[20] L. TABER, *Large deflection of a fluid-filled spherical shell under a point load,* J. Appl. Mech., 49 (1982), pp. 121-127.

[21] Y. H. LIN AND F. Y. M. WAN, *Asymptotic analysis of steadily spinning shallow caps under uniform pressure,* IAMS Tech. Rep. No. 83-26, Univ. British Columbia, Vancouver, Dec. 1983.